

1 SEARCH FOR PRODUCTION OF A HIGGS BOSON AND A SINGLE TOP
2 QUARK IN MULTILEPTON FINAL STATES IN PP COLLISIONS AT $\sqrt{S} = 13$
3 TEV

4 by

5 Jose Andres Monroy Monta  ez

6 A DISSERTATION

7 Presented to the Faculty of

8 The Graduate College at the University of Nebraska

In Partial Fulfilment of Requirements

10 For the Degree of Doctor of Philosophy

11 Major: Physics and Astronomy

12 Under the Supervision of Kenneth Bloom and Aaron Dominguez

13 Lincoln, Nebraska

14 July, 2018

15 SEARCH FOR PRODUCTION OF A HIGGS BOSON AND A SINGLE TOP
16 QUARK IN MULTILEPTON FINAL STATES IN PP COLLISIONS AT $\sqrt{S} = 13$

17 TEV

18 Jose Andres Monroy Montañez, Ph.D.

19 University of Nebraska, 2018

20 Adviser: Kenneth Bloom and Aaron Dominguez

²¹ Table of Contents

²² Table of Contents	iii
²³ List of Figures	vi
²⁴ List of Tables	ix
²⁵ 1 INTRODUCTION	1
²⁶ 2 Theoretical approach	2
27 2.1 Introduction	2
28 2.2 Standard Model of particle physics	4
29 2.2.1 Gauge Bosons	7
30 2.2.2 Fermions	9
31 2.2.2.1 Leptons	10
32 2.2.2.2 quarks	13
33 2.3 Electroweak unification and the Higgs mechanism	17
34 2.3.1 Spontaneous symmetry breaking	25
35 2.3.2 Higgs mechanism	29
36 2.3.3 Masses of the gauge bosons	31
37 2.3.4 Masses of the fermions	32

38	2.3.5 The Higgs field	33
39	2.4 The tHq process	37
40	2.5 The CP phase	37
41	3 The CMS experiment at the LHC	38
42	3.1 The LHC	39
43	3.2 The CMS experiment	42
44	4 Search for production of a Higgs boson and a single top quark in	
45	multilepton final states in pp collisions at $\sqrt{s} = 13$ TeV	44
46	4.1 Introduction	44
47	4.2 Data and MC Samples	45
48	4.2.1 Full 2016 dataset and MC samples	46
49	4.2.2 Triggers	46
50	4.2.2.1 Trigger efficiency scale factors	49
51	4.3 Object Identification and event selection	50
52	4.3.1 Jets and b tagging	50
53	4.3.2 Lepton selection	50
54	4.3.3 Lepton selection efficiency	52
55	4.4 Background predictions	53
56	4.5 Signal discrimination	54
57	4.5.1 Classifiers response	57
58	4.6 Additional discriminating variables	60
59	5 The CMS forward pixel detector	64
60	5.0.1 The phase 1 FPix upgrade	64
61	5.0.2 FPix module production line	64

62	5.0.3	The Gluing stage	64
63	5.0.4	The Encapsulation stage	64
64	5.0.5	The FPix module production yields	64
65	Bibliography		64
66	References		65

⁶⁷ List of Figures

68	1.1	^{14}N neutron capture in a PECVD polymerized pyridine film. The Q-value of this reaction is 626 keV. Taken from [22]	1
70	2.1	Fundamental interactions in nature.	5
71	2.2	Standard model of particle physics.	8
72	2.3	Leptons interactions	11
73	2.4	WI transformations between quarks	15
74	2.5	Neutral current processes	18
75	2.6	Spontaneous symmetry breaking mechanism	26
76	2.7	SSB Potential form	26
77	2.8	Potential for complex scalar field	27
78	2.9	SSB mechanism for complex scalar field	28
79	2.10	Higgs production mechanism Feynman diagrams	34
80	2.11	Higgs production cross section and decay branching ratios	35
81	3.1	ref. C.Lefevre, “The CERN accelerator complex,” (2008). CERN-DI- 0812015.	40

83	3.2	ref. J.-L. Caron , “Layout of the LEP tunnel including future LHC in-	
84		frastructures.. L’ensemble du tunnel LEP avec les futures infrastructures	
85		LHC!”, https://cds.cern.ch/record/841542 (Nov, 1993). AC Collection.	
86		Legacy of AC. Pictures from 1992 to 2002..	41
87	3.3	ref. ACTeam, “Diagram of an LHC dipole magnet. Schéma d’un aimant	
88		dipôle du LHC,” (1999). CERN-DI-9906025.	42
89	3.4	ref: CMS Collaboration, “Detector Drawings”, CMS-PHO-GEN-2012-002,	
90		http://cds.cern.ch/record/1433717 , 2012.	43
91	4.1	The two leading-order diagrams of tHq production.	45
92	4.2	Distributions of input variables to the BDT for signal discrimination, three	
93		lepton channel, normalized to their cross section and to 35.9fb^{-1}	55
94	4.3	Distributions of input variables to the BDT for signal discrimination, three	
95		lepton channel.	57
96	4.4	BDT inputs as seen by TMVA (signal, in blue, is tHq , background, in	
97		red, is $t\bar{t}$) for the three lepton channel, discriminated against $t\bar{t}$ (fakes)	
98		background.	58
99	4.5	BDT inputs as seen by TMVA (signal, in blue, is tHq , background, in	
100		red, is $t\bar{t}W+t\bar{t}Z$) for the three lepton channel, discriminated against $t\bar{t}V$	
101		background.	59
102	4.6	Signal (left), $t\bar{t}$ background (middle), and $t\bar{t}V$ background (right.) corre-	
103		lation matrices for the input variables in the TMVA analysis for the three	
104		lepton channel.	60

¹¹³ List of Tables

114	2.1	Gauge Bosons.	9
115	2.2	Fermions of the SM.	10
116	2.3	Leptons properties.	13
117	2.4	Quarks properties.	14
118	2.5	Fermion multiplets weak isospin and weak hypercharge.	16
119	2.6	Higgs boson properties.	33
120	2.7	The SM Higgs boson production cross sections for $m_H = 125\text{GeV}/c^2$.	35
121	2.8	The branching ratios for a SM Higgs boson with $m_H = 125\text{GeV}/c^2$.	36
122	4.1	Signal samples and their cross section and branching fraction used in this analysis. See Ref. [40] for more details.	46
123			
124	4.2	κ_V and κ_t combinations generated for the two signal samples and their NLO cross sections. The tHq cross section is multiplied by the branching fraction of the enforced leptonic decay of the top quark (0.324). See also Ref. [40].	47
125			
126			
127			

128	4.3	List of background samples used in this analysis (CMSSW 80X). In the 129 first section of the table are listed the samples of the processes for which 130 we use the simulation to extract the final yields and shapes, in the second 131 section the samples of the processes we will estimate from data. The 132 MC simulation is used to design the data driven methods and derive the 133 associated systematics.	48
134	4.4	Leading-order $t\bar{t}W$ and $t\bar{t}Z$ samples used in the signal BDT training. . .	48
135	4.5	Table of high-level triggers that we consider in the analysis.	49
136	4.6	Trigger efficiency scale factors and associated uncertainties, shown here 137 rounded to the nearest percent.	50
138	4.7	Requirements on each of the three muon selections. In the cases where 139 the cut values change between the selections, those values are listed in the 140 table. Otherwise, whether the cut is applied is indicated. For the two 141 p_T^{ratio} and CSV rows, the cuts marked with a † are applied to leptons that 142 fail the lepton MVA cut, while the loose cut value is applied to those that 143 pass the lepton MVA cut.	51
144	4.8	Criteria for each of the three electron selections. In cases where the cut 145 values change between selections, those values are listed in the table. 146 Otherwise, whether the cut is applied is indicated. In some cases, the 147 cut values change for different η ranges. These ranges are $0 < \eta < 0.8$, 148 $0.8 < \eta < 1.479$, and $1.479 < \eta < 2.5$ and the respective cut values are 149 given in the form (value ₁ , value ₂ , value ₃).	52
150	4.9	MVA input discriminating variables	56
151	4.10	TMVA input variables ranking for BDTA_GRAD method for the trainings 152 in the three lepton channel. For both trainings the rankings show almost 153 the same 5 variables in the first places.	61

154	4.11 TMVA configuration used in the BDT training.	61
155	4.12 ROC-integral for all the testing cases we made in the evaluation of the	
156	additional variables discriminating power. The improvement in the dis-	
157	crimination performance provided by the additional variables is about 1%	
158	63

¹⁵⁹ Chapter 1

¹⁶⁰ INTRODUCTION

Figure 1.1: ^{14}N neutron capture in a PECVD polymerized pyridine film. The Q-value of this reaction is 626 keV. Taken from [22]

¹⁶¹ Chapter 2

¹⁶² Theoretical approach

¹⁶³ Introduction

¹⁶⁴ The physical description of the universe is a challenge that physicist have faced by
¹⁶⁵ making theories that refine the existing principles and proposing new ones in an
¹⁶⁶ attempt to embrace emerging facts and phenomena. By early 1800's, there were sep-
¹⁶⁷ arate theories describing electric and magnetic phenomena, gravitational force and
¹⁶⁸ light. The invention of the electric battery by Alessandro Volta about 1800, the dis-
¹⁶⁹ covery of the magnetic effects of the electric current by Oersted and Ampere (1820)
¹⁷⁰ and the generation of electric current using changing magnetic fields by Faraday
¹⁷¹ (1831), represent the first steps in the way to create a unified theory of electromag-
¹⁷² netism. The unification was carried out by James Clerk Maxwell who was able to
¹⁷³ put together electricity and magnetism in a set of 20 equations known as "general
¹⁷⁴ equations of the electromagnetic field", relating the observables that describes the
¹⁷⁵ experimental laws of the electromagnetism. By combining these equations, Maxwell
¹⁷⁶ found a wave equation and propose the existence of the "electromagnetic waves". The
¹⁷⁷ calculation of the propagation speed of the electromagnetic waves turned out to be
¹⁷⁸ the same as the speed of light, therefore, the natural conclusion was that light is an

179 electromagnetic wave. By that time, waves were consider a perturbation of a ma-
180 terial medium which in the case of the electromagnetic waves was identified as the
181 “*Luminiferous Ether*”.

182 By 1900, Max Plank came out with the idea that radiation is quantized and Albert
183 Einstein in 1905 made use of that hypothesis to propose the existence of the light
184 quantum, the “*photon*”, in order to explain the photoelectric effect [1] . The well-
185 known quantum revolution in physics started and the particle-wave duality of photons
186 arose as a natural behavior later extended to electrons and to all kind of particles
187 in nature. The development of a quantum theory, allowed to explain a set of, at
188 than time, non-common sense effects like the quantum tunneling and the prediction
189 of some other exotic phenomena like the quantum entanglement, however, quantum
190 theory was separated from the recently unified electromagnetism.

In 1905, Einstein also published two more papers: one aimed to describe his statistical molecular theory of liquids and how it can be used to describe the brownian motion [2]. At that time the existence of the atoms and molecules were not fully demonstrated but Einstein’s theory provided an explanation as well as predictions based on the their existence. Jean Perrin in 1908 conducted experiments that confirmed Einstein’s predictions. The other paper was directed to describe the space and time relationship [3], unifying the notion of space and time into one entity known as “*spacetime*” that treats space and time at the same level and then discarding the absoluteness of time. The new theory known as special relativity, supersedes the Galilean relativity principle and postulate exceptional effects like the time dilation, length contraction and mass-energy equivalence through the most famous formula in physics [4]

$$E = mc^2$$

191 The generalization of the special relativity was presented in 1916 and includes a gener-
 192 alization of the Newton's law of universal gravitation, becoming a unified description
 193 of gravity as a geometric property of space and time. Einstein's predictions includes
 194 the existence of black holes and the recently observed, by LIGO collaboration, "*grav-*
 195 *itational waves*".

196 At the end od 1940s, based in the work of Sin-Itiro Tomonaga [5], Julian Schwinger [6]
 197 and Richard P. Feynman [7] developed an electromagnetic theory consistent with the
 198 special relativity and quantum mechanics that describes how matter and light inter-
 199 acts; the so-called "quantum eletrodynamic" (QED) had born. Despite the incredible
 200 success of the general relativity describing the macroworld where gravity dominates
 201 and quantum mechanics describing the microworld where other forces dominates, a
 202 self-consistent theory of quantum gravity is not yet available.

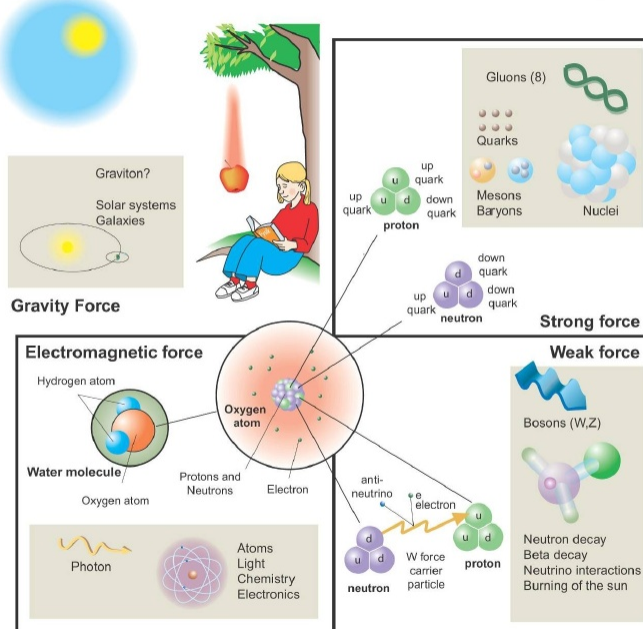
203 Standard Model of particle physics

204 Even though there are many manifestations of force in nature, we can reduce all of
 205 them to one of four fundamental interactions represented in the figure 2.1:

- 206 • *Electromagnetic interaction (EMI)* affect particles "electrically charged", like
 207 electrons and protons. It is described by QED combining quantum mechanics,
 208 special relativity and electromagnetism in order to explain how particles with
 209 electric charge interact through the exchange of photons, therefore, one says
 210 that "Electomagnetic Force" is mediated by "photons".
- 211 • *Strong interaction (SI)* described by Quantum Chromodynamics (QCD). Elec-
 212 trons and photons are examples of elementary particles, since they have no
 213 internal structure, but protons, neutrons and a bunch of other particles have it.

Fundamental interactions.

Illustration: Typoform



Summer School KPI 15 August 2009

Figure 2.1: Fundamental interactions in nature. Despite the many manifestations of forces in nature, we can track all of them back to one of the fundamental interactions. The most common forces are gravity and electromagnetic given that all of us are subject and experience them in the normal life. Image taken from <https://www.slideshare.net/ssakpi/study-of-the-antimatter-at-large-hadron-collider>

214 They are called hadrons and are composed of two or more valence quarks¹ which
 215 are elementary particles. Quarks have fractional electric charge which means
 216 that they are subject to electromagnetic interaction; however, they are held
 217 together inside the hadrons against their electrostatic repulsion by the “Strong
 218 Force” through the exchange of “gluons”. The equivalent to the electric charge
 219 is the “color charge” which comes in three varieties: Red, Blue and Green.

- 220 • *Weak interaction (WI)* described by the Weak theory (WT), is responsible for
 221 instance for the radioactive decay in atoms, nuclear fission and fusion. Quarks
 222 and leptons are the particles affected by the weak interaction and possess a

¹ particles made of four and five quarks are exotic states not so common

223 property called “flavor charge” which can be changed by emitting or absorbing
 224 one weak force mediator; they comes in six flavors each (see 2.2.2). There
 225 are three mediators of the “Weak force” known as “Z” boson in the case of
 226 electrically neutral changes and “ W^\pm ” bosons in the case of electrically charged
 227 changes. The “weak isospin” is the WI analog to electric charge in EMI and
 228 color charge in SI and define how quarks and leptons are affected by the weak
 229 force. Since this thesis is in the frame of electroweak interaction, a more detailed
 230 description of it will be given in section 2.3

231 • *Gravitational interaction (GI)* described by General Theory of Relativity (GR).
 232 It is responsible for the structure of galaxies and other large-scale structures
 233 like black holes as well as the expansion of the universe. As a classical theory,
 234 in the sense that it can be formulated without even appeal to the concept of
 235 quantization, it implies that the spacetime is a continuum and predictions can
 236 be made without limitation to the precision of the measurement tools which
 237 represent a direct contradiction of the quantum mechanics principles. Gravity
 238 is deterministic while quantum mechanics is probabilistic; despite that, efforts
 239 to develop a quantum theory of gravity have come out with the “graviton” as
 240 mediator of the Gravitational force².

241 Quantum field theory (QFT) is the theoretical framework for building quantum me-
 242 chanical models that describes particles and their interactions. It is composed of a set
 243 of mathematical tools that combines classical fields, special relativity, and quantum
 244 mechanics while keeping the quantum point particles and locality ideas. Currently,
 245 particle physics at the fundamental level is modeled in terms of a collection of particles
 246 and fields in a theory known as the “Standard model of particle physics (SM)”.

² Actually a wide variety of theories have been developed in an attempt to describe gravity; some famous examples are the string theory and supergravity

247 The mathematical formulation of the SM is based on group theory³ and the use of
 248 the Noether's theorem [11].

249 The symmetry group $SU(3)_C \otimes SU(2)_L \otimes U(1)_Y$ describes strong, weak and elec-
 250 tromagnetic interactions in terms of symmetries associated to physical quantities:

251 • $SU(3)_C$ associated to color charge

252 • $SU(2)_L$ associated to weak isospin and chirality

253 • $U(1)_Y$ associated to weak hypercharge and electric charge

254 It will be shown that the electromagnetic and weak interactions are combined in
 255 the so-called electroweak interaction where chirality, hypercharge, weak isospin and
 256 electric charge are the central concepts.

257 The full picture of the SM is composed of three fields⁴, whose excitations are in-
 258 terpreted as particles called mediators or force-carriers, a set of elementary particles
 259 interacting through the exchange of those mediators and a field that give the mass of
 260 elementary particles (see Fig. 2.2).

261 Gauge Bosons

262 As was mentioned above, the importance of the “gauge bosons” falls in the fact
 263 that they are the force mediators or force carriers. All of them are spin-1 particles,
 264 therefore classified as bosons since they obey the Bose-Einstein statistics.

265 The features of the gauge bosons reflects the features of the fields they represent. In
 266 the case of electromagnetic force the interaction occurs when the photon is exchanged

³ The formal and complete treatment of the SM is out of the scope of this document, however a plenty of textbooks describing it at several levels are available in the literature. The treatment in “An Introduction To Quantum Field Theory (Frontiers in Physics)” by Michael E. Peskin and Dan V. Schroeder is quite comprehensive and detailed.

⁴ Note that gravitational field is not included in the standard model formulation

Standard Model of Elementary Particles

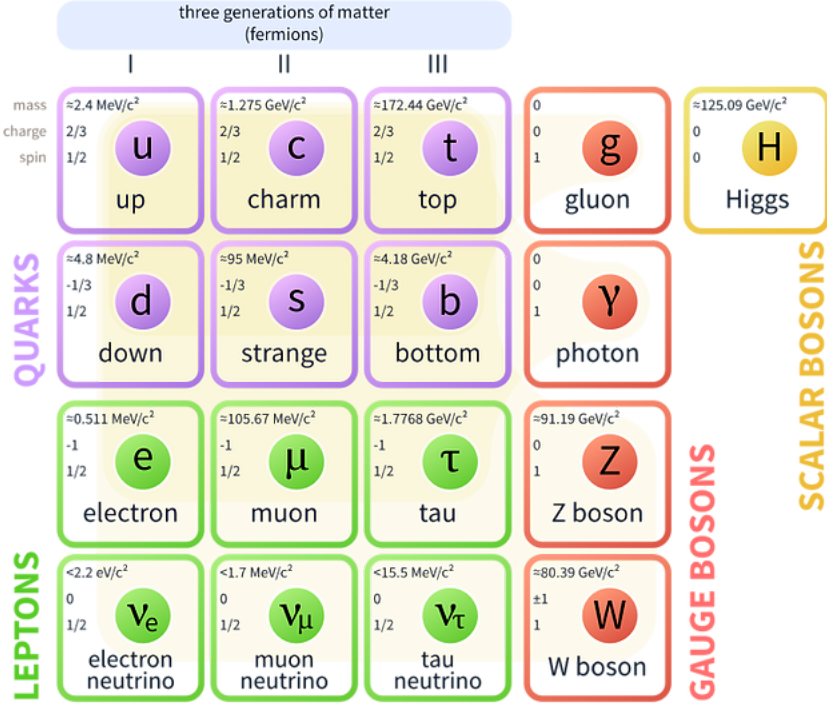


Figure 2.2: Schematic representation of the Standard model of particle physics. SM is a theoretical model intended to describe three of the four fundamental force of the universe in terms of a set of particles and their interactions. Additionally to the particles in the scheme, their corresponding anti-particles, with opposite quantum numbers, are also part of the picture; some particles are their own anti-particles, like photon or Higgs, or anti-particle is already listed like in the W^+ and W^- case. Image taken from <https://www.collegiate-advanced-electricity.com/single-post/2017/04/10/The-Standard-Model-of-Particle-Physics>.

- 267 between (couples to) particles carrying electric charge; however, the photon itself does
 268 not carry electric charge which added to the fact that it is massless means that there
 269 is not coupling between photons and that the EMI is of infinite range i.e. particles
 270 electrically charged interacts even if they are located far away one from each other.
 271 In the case of the SI, gluons are massless, like photons, but they carry one unit of
 272 color charge and one unit of anticolor charge which means that gluons couples to other
 273 gluons. As a result, the range of the SI is not infinite but very short (see table 2.1) due
 274 to the attraction between gluons, giving rise to the “color confinement” which explain

275 why color charged particles cannot be isolated but live within composed particles, like
 276 quarks inside protons.

277 The WI mediators, W^\pm and Z, are massive which explain WI short-range. Given that
 278 the WI is the only interaction that can change the flavor of the interacting particles,
 279 the W boson is the responsible for the nuclear transmutation where a neutron is
 280 converted in a proton or vice versa with the involvement of an electron and a neutrino.
 281 On the other side, the Z boson is the responsible of the neutrino elastic scattering
 282 where no electric charge but momentum transference is involved. Table 2.1 summarize
 283 the main features of the gauge bosons and fundamental interactions.

Interaction	Acts on	Relative strength	Range (m)	Mediators	Mediator mass (GeV/c^2)
Electromagnetic (QED)	Electrically charged particles	10^{-2}	Infinite	Photon	0
Strong (QCD)	Quarks and gluons	1	10^{-15}	Gluon	0
Weak (WI)	Leptons and quarks	10^{-6}	10^{-18}	W^\pm, Z	$m_W = 91.2$ $m_Z = 80.4$
Gravitational (GI)	Massive particles	10^{-39}	Infinite	Graviton	0

Table 2.1: Gauge bosons and fundamental interactions features.

284

285 Fermions

286 The set of elementary particles involved in the SM formulation are quarks and leptons,
 287 being them the basic constituents of the ordinary matter at the lowest level. All of
 288 them have spin 1/2, therefore they are classified as fermions since they obey the
 289 Fermi-Dirac statistics. In both cases, they come in six flavors and are organized in
 290 three generations or families as shown in the table 2.2.

291

		Generation		
Type		1st	2nd	3rd
Leptons	Charged	Electron (e)	Moun(μ)	Tau (τ)
	Neutral	Electron neutrino (ν_e)	Muon neutrino (ν_μ)	Tau neutrino (ν_τ)
Quarks	Up-type	Up (u)	Charm (c)	Top (t)
	Down-type	Down (d)	Starnge (s)	Bottom (b)

Table 2.2: Fermions of the SM. Quarks and leptons comes in six flavors each and are organized in three generations or families composed of two pairs of closely related particles. Generations differs by mass and flavor quantum numbers but share interactions.

292 There is a mass hierarchy between generations where the higher generation particles
 293 decays to the lower one which can explain why the ordinary matter is made of particles
 294 in the first generation. In the SM, neutrinos are modeled as massless particles so they
 295 are not subject to this mass hierarchy; however, today it is known that neutrinos
 296 are massive so the hierarchy could be restated. The second and third generation
 297 fermions are produced in high energy processes, like the ones recreated in the particles
 298 accelerators.

299 Leptons

300 A lepton is an elementary particles that is not subject to the SI. As seen in table 2.2,
 301 there are two types of leptons, the charged ones (electron, muon and tau) and the
 302 neutral ones (the three neutrinos). The electric charge (Q) is the property that gives
 303 leptons the ability to participate of the EI. Since the classical point of view, Q plays
 304 a central role determining, among others, the strength of the electric field through
 305 which the electromagnetic force is exerted.

306 In QED, Q operator is the generator of the U(1) symmetry which according to the
 307 Noether's theorem means that there is a conserved charge; this conserved charge is
 308 the electric charge and thus the law conservation of electric charge is stated. It is
 309 clear that neutrinos are not affected by EI because they don't carry electric charge.

310 The interaction with the gauge field involves only one kind of lepton i.e. at the vertex
 311 both lepton lines refers to the same kind of lepton (see fig. 2.3), therefore EI does
 312 not change flavor; actually a new quantum number was defined out of that fact, the
 313 so-called “Lepton number” was assigned to each lepton flavor:

314 • Electron number: $N_e = N(e^-) - N(e^+)$

315 • Muon number : $N_\mu = N(\mu^-) - N(\mu^+)$

316 • Tau number : $N_\tau = N(\tau^-) - N(\tau^+)$

317 representing the number of leptons plus the number of anti-leptons of each flavor
 318 entering in a process. These quantum numbers are conserved in EI and SI since they
 319 don't change flavor.

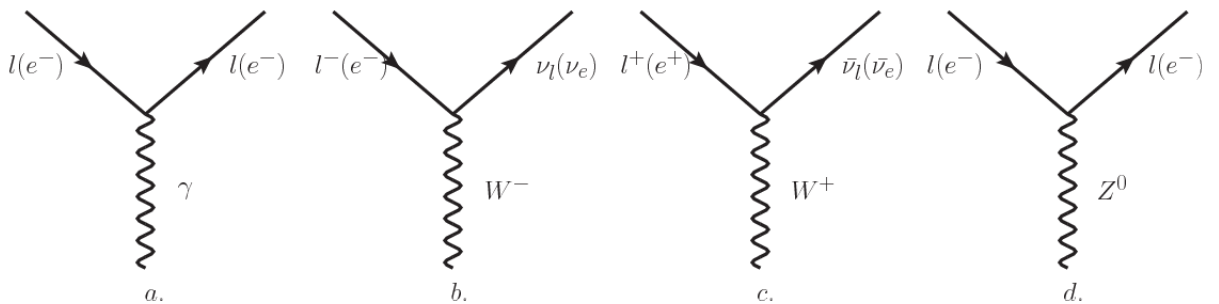


Figure 2.3: Diagrams representing the leptons interactions with the gauge fields; a: EI-electron and photon; b,c,d: WI - first generation leptons.

320 Another feature of the leptons that is fundamental in the mathematical description
 321 of the SM is the chirality which is closely related to spin and helicity. Helicity de-
 322 fine the handedness of a particle by relating its spin and momentum such that if
 323 they are parallel then the particle is right-handed; if spin and momentum are an-
 324 tiparallel the particle is said to be left-handed. The study of parity conservation (or
 325 violation) in β -decay have shown that only left-handed electrons/neutrinos or right-
 326 handed positrons/anti-neutrinos are created [12]; The inclusion of that feature in the

theory was seeked out by using projection operators for helicity, however, helicity is frame dependent for massive particles which makes it not Lorentz invariant and then another related attribute has to be used: *Chirality*. Chirality is a purely quantum attribute which makes it not so easy to describe in graphical terms but it defines how the wave function of a particle transform under certain rotations. Same as helicity, there are two chiral states, left-handed chiral (L) and right-handed chiral(R). In the highly relativistic limit where $E \approx p \gg m$ helicity and chirality converge becoming exactly the same for massless particles. In the following when referring to left-handed (right-handed) it means left-handed chiral (right-handed chiral). The fundamental fact about chirality is that while for QED and QCD are not sensible to chirality, in WI left-handed and right-handed fermions are treated asymmetrically, such that only left handed fermions and right-handed anti-fermions are allowed to couple to weak gauge bosons, which is a violation of the Parity. The way to translate this statement in a formal mathematical formulation is based on the isospin symmetry group $SU(2)_L$. Each generation of leptons is seen as a weak isospin doublet.⁵ The left-handed charged lepton and its associated left-handed neutrino are arranged in doublets of weak isospin $T=1/2$ while their right-handed partners are singlets:

$$\begin{pmatrix} \nu_l \\ l \end{pmatrix}_L, l_R := \begin{pmatrix} \nu_e \\ e \end{pmatrix}_L, \begin{pmatrix} \nu_\mu \\ \mu \end{pmatrix}_L, \begin{pmatrix} \nu_\tau \\ \tau \end{pmatrix}_L, e_R, \mu_R, \tau_R, \nu_{eR}, \nu_{\mu R}, \nu_{\tau R} \quad (2.1)$$

The Isospin third component refers to the eigenvalues of the weak isospin operator which for doublets is $T_3 = \pm 1/2$, while for singlets it is $T_3 = 0$. The physical meaning of this doublet-singlet arrangement falls in that the WI couples the two particles in the doublet by exchanging the interaction mediator while the singlet member is not involved in WI.

⁵ The weak isospin is an analogy of the isospin symmetry in strong interaction where neutron and proton are affected equally by strong force but differ in its charge.

349 Lepton number definition has to be extended when considering the WI. The new
 350 definition is given in terms of the generation's weak isospin doublets, thus, electron
 351 and electron neutrino have electron number $L_e = 1$, muon and muon neutrino have
 352 muon number $L_\mu = 1$, tau and tau neutrino have tau number $L_\tau = 1$. Lepton number
 353 conservation, which now is SM wide, implies that leptons have to be created in pairs
 354 with their anti-leptons. The main properties of the leptons are summarized in the
 355 table 2.3.

356 Altough all three flavor neutrinos have been observed, their masses remain unknown
 357 and only some estimations have been made [13]. The main reason being that the flavor
 358 eigenstates are not the same as the mass eigenstates which imply that when a neutrino
 359 is created its mass state is a linear combination of the three mass eigenstates. The
 360 Pontecorvo-Maki-Nakagawa-Sakata (PMNS) mixing matrix encode the relationship
 361 between flavor and mass eigenstates.

Lepton	$Q(e)$	T_3	L_e	L_μ	L_τ	Mass (MeV/C^2)	Lifetime (s)
Electron (e)	-1	-1/2	1	0	0	0.5109989461(31)	Stable
Electron neutrino(ν_e)	0	1/2	1	0	0	Unknown	Unknown
Muon (μ)	-1	-1/2	0	1	0	105.6583745(24)	$2.1969811(22) \times 10^{-6}$
Muon neutrino (ν_μ)	0	1/2	0	1	0	Unknown	Unknown
Tau (τ)	-1	-1/2	0	0	1	1776.86(12)	$290.3(5) \times 10^{-15}$
Tau neutrino (τ_μ)	0	1/2	0	0	1	Unknown	Unknown

Table 2.3: Leptons properties; Q:Electric charge, T_3 :Weak isospin. Only left-handed leptons and right-handed anti-leptons participate of the WI. Anti-particles with inverted T_3 , Q and lepton number complete the leptons set but are not listed. Right-handed leptons and letf-handed anti-leptons, neither listed, form weak isospin singlets with $T_3 = 0$ and do not take part in the weak interaction.

362

363 quarks

364 Quarks are the basic constituents of protons, neutrons and other non-elementary
 365 particles. The way quarks join to form bound states, called hadrons, is through the

366 strong interaction mediated by gluons. Quarks are affected by all the fundamental
 367 interactions which means that they carry all the four types of charges: Color, electric
 368 charge, weak isospin and mass. Table 2.4 summarize quarks features, among which
 369 the most particular is their fractional electric charge. Note that fractional charge is
 370 not a problem, given that quarks are not found isolated, but serve to explain how
 371 composed particles are formed out of two or more valence quarks⁶.

Flavor	Q(e)	I_3	T_3	B	C	S	T	B'	Y	Color	Mass (MeV/C^2)
Up (u)	2/3	1/2	1/2	1/3	0	0	0	0	1/3	r,b,g	$2.2^{+0.6}_{-0.4}$
Charm (c)	2/3	0	1/2	1/3	1	0	0	0	4/3	r,b,g	$1.28 \pm 0.03 \times 10^3$
Top(t)	2/3	0	1/2	1/3	0	0	1	0	4/3	r,b,g	$173.1 \pm 0.6 \times 10^3$
Down(d)	-1/3	-1/2	-1/2	1/3	0	0	0	0	1/3	r,b,g	$4.7^{+0.5}_{-0.4}$
Strange(s)	-1/3	0	-1/2	1/3	0	-1	0	0	-2/3	r,b,g	96^{+8}_{-4}
Bottom(b)	-1/3	0	-1/2	1/3	0	0	0	-1	-2/3	r,b,g	$4.18^{+0.04}_{-0.03} \times 10^3$

Table 2.4: Quarks properties. Q: Electric charge, I_3 : Isospin, T_3 : Weak isospin, B:Baryon number, C:Charmness, S:strangeness, T:topness, B':Bottomness, Y: Hypercharge. Anti-quarks posses the same mass and spin as quarks but all charges (color, flavor numbers) have opposite sign.

372

373 Color charge is the responsible for the SI between quarks and is the symmetry
 374 ($SU(3)_C$) that define QCD. There are three colors: red (r), blue(b) and green(g) and
 375 their corresponding three anti-colors; thus each quark carries one color unit while
 376 anti-quarks carries one anti-color unit. As said above, quarks are not allowed to be
 377 isolated due to the color confinement effect, therefore its features have been studied
 378 indirectly by observing their bound states created when:

- 379 • one quark with a color charge is attracted by an anti-quark with the correspond-
 380 ing anti-color charge forming a colorless particle called “meson”.

⁶ Hadrons can contain an indefinite number of virtual quarks and gluons, known as the quark and gluon sea, but only the valence quarks determine hadrons' quantum numbers.

381 • three quarks(anti-quarks) with different color(anti-color) charges are attracted
 382 among them forming a colorless particle called “baryon(anti-baryon)”.

383 In the first version of the quark model (1964), M. Gell-Mann [14] and G. Zweig [15,16]
 384 developed a consistent way to classify hadrons according to their properties. Only
 385 three quarks (u, d, s) were involved in a scheme in which all baryons have baryon
 386 number $B=1$ and therefore quarks have $B=1/3$; all the rest of particles have $B=0$.
 387 The scheme organize the baryons in a two-dimensional space ($I_3 - Y$) where Y (is
 388 known as Hypercharge) and I_3 (isospin) are quantum numbers related by the Gell-
 389 Mann-Nishijima formula [17,18]:

$$Q = I_3 + \frac{Y}{2} \quad (2.2)$$

390 where $Y = B + S + C + T + B'$ are the quantum numbers listed in table 2.4. Baryon
 391 number is conserved in SI and EI which means that single quarks cannot be created
 392 but in pairs $q - \bar{q}$.

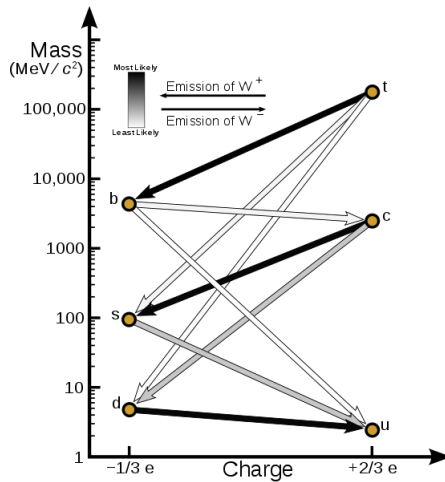


Figure 2.4: Transformations between quarks through WI. Higher generations quarks decay to first generation quarks by emitting a W boson. The arrow color indicate the likelihood of the transition according to the grey scale in the top left side which represent the CKM matrix parameters [19].

393 Similar to leptons, there are six quark flavors organized in three generations (see table
 394 2.2) and following a mass hierarchy which again implies that higher generations decay
 395 to first generation quarks. Figure 2.4 show a diagram representing the weak trans-
 396 formations between quarks. Note that quark decays are greatly favoured between
 397 generation members.

Quarks				T_3	Y_W
Doublets	$(\begin{smallmatrix} u \\ d' \end{smallmatrix})_L$	$(\begin{smallmatrix} c \\ s' \end{smallmatrix})_L$	$(\begin{smallmatrix} t \\ b' \end{smallmatrix})_L$	$(\begin{smallmatrix} 1/2 \\ -1/2 \end{smallmatrix})$	1/3
Singlets	u_R	c_R	t_R	0	4/3
Leptons					
Doublets	$(\begin{smallmatrix} \nu_e \\ e \end{smallmatrix})_L$	$(\begin{smallmatrix} \nu_\mu \\ \mu \end{smallmatrix})_L$	$(\begin{smallmatrix} \nu_\tau \\ \tau \end{smallmatrix})_L$	$(\begin{smallmatrix} 1/2 \\ -1/2 \end{smallmatrix})$	-1
Singlets	ν_{eR}	$\nu_{\mu R}$	$\nu_{\tau R}$	0	-2

Table 2.5: Fermion multiplets weak isospin and weak hypercharge. Weak hypercharge is calculated using the Gell-Mann-Nishijima formula.

398

399 Actually, the isospin doublets of quarks are also defined (see table 2.5) but this time
 400 one has to consider that there are inter-generations couplings i.e. members of different
 401 quark generations are connected by the WI mediator but for leptons the transforma-
 402 tion is limited to members of the same generation, thus up-type quarks are coupled not
 403 to down-type quarks directly but to a superposition of down-type quarks (q'_d) via WI.
 404 The weak decays are then described according to the Cabibbo-Kobayashi-Maskawa
 405 (CKM) mixing matrix [20, 21]:

$$\begin{aligned}
 q'_d &= V_{CKM} q_d \\
 406 \quad \begin{pmatrix} d' \\ s' \\ b' \end{pmatrix} &= \begin{pmatrix} V_{ud} & V_{us} & V_{ub} \\ V_{cd} & V_{cs} & V_{cb} \\ V_{td} & V_{ts} & V_{tb} \end{pmatrix} \begin{pmatrix} d \\ s \\ b \end{pmatrix} \tag{2.3}
 \end{aligned}$$

407 V_{CKM} is a 3×3 unitary matrix, parametrized by three mixing angles and the CP -
 408 *mixing phase*; the latter is the parameter responsible for the CP-violation in the SM.
 409 Weak hypercharge is calculated through the Gell-Mann-Nishijima formula 2.2 but
 410 using the weak isospin and charge for quarks (table 2.5). It will be shown that weak
 411 hypercharge is one of the symmetries used in the electroweak unification.

412 Electroweak unification and the Higgs mechanism

413 Physicist dreams with building a theory that contains all the interactions in one single
 414 interaction, i.e. showing that at some scale in energy all the four fundamental interac-
 415 tions are unified and only one interaction emerges in a “Theory of everything”. First
 416 sign of the feasibility of such unification comes from success in the construction of the
 417 QED. Einstein spent years trying to reach that dream, which by 1920 only involved
 418 electromagnetism and gravity, with no success; however, a new partial unification was
 419 achieved in the 1960’s, when S.Glashow [8], A.Salam [9] and S.Weinberg [10] indepen-
 420 dently proposed that electromagnetic and weak interactions are two manifestations
 421 of a more general interaction called “electroweak interaction”. QCD and EWT were
 422 developed in parallel and following the useful prescription provided by QED and the
 423 gauge invariance principles.

424 The theory of weak interactions was capable to explain the $\beta - decay$ and in general
 425 the weak charged currents like the ones present in processes b and c of the figure 2.3
 426 which now can be extended to currents involving quarks and known as charged fermion
 427 currents; therefore, fermion doublets are coupled by W^\pm bosons⁷. However, there
 428 were some processes like the “ $\nu_\mu - e$ scattering” which would require the exchange of
 429 two W bosons (see figure 2.5 top diagrams) and give rise to divergent loop integrals.

⁷ This implies that these fermion doubles are also the decay channels of the W^\pm bosons

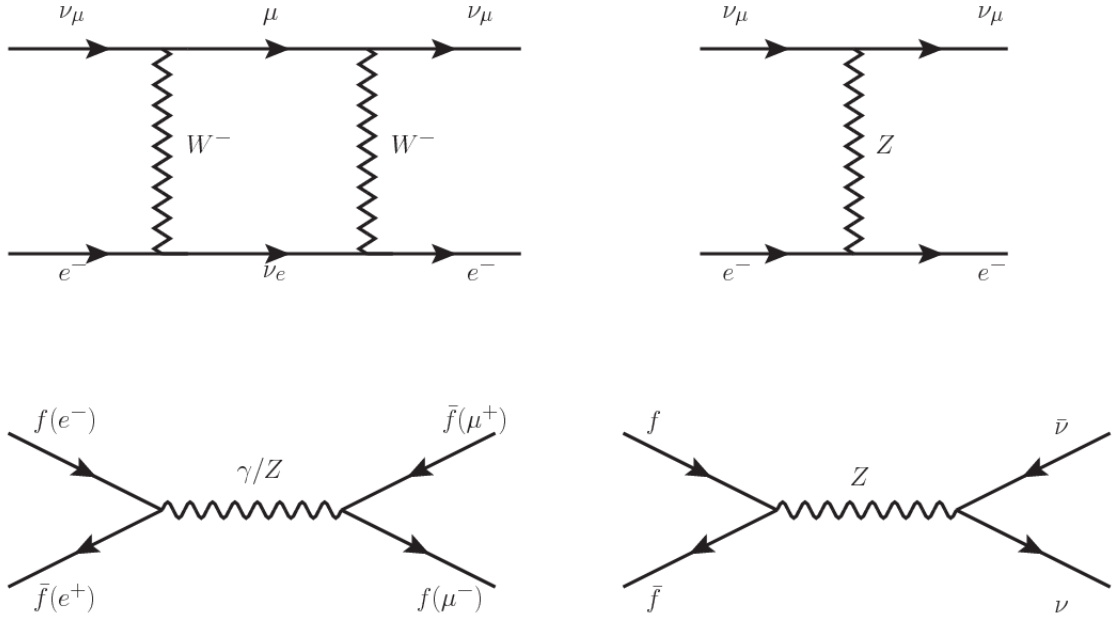


Figure 2.5: [Top: $\nu_\mu - e^-$ scattering going through charged currents(left) and neutral currents(right). Bottom: neutral current processes for charged fermions(left) and involving neutrinos(right). While neutral current processes involving only charged fermions can proceed through EI or WI, those involving neutrinos can only proceed via WI. The former can be seen as an indication that at some level WI and EI are closely connected.

- 430 The neutral currents involving fermions via the exchange of a neutral boson Z , makes
 431 up the needed extension. Neutral weak interaction vertices conserve flavor in the
 432 same way as the electromagnetic vertices does, but Z boson can couple to neutrinos
 433 which imply that processes involving charged fermions can proceed through EI or WI
 434 but processes involving neutrinos can proceed only through WI.
 435 The prescription to build a gauge theory of the WI consist in proposing a free field
 436 lagrangian density that includes the particles involved; next, by requesting invariance
 437 under global phase transformations first and generalizing to local phase transfor-
 438 mations invariance later, the conserved currents are identified and interactions are
 439 generated by introducing gauge fields. Given that the goal is to include the EI and
 440 WI in a single theory, the group symmetry considered should be a combination of

441 $SU(2)_L$ and $U(1)_{em}$, however the later cannot be used directly because the EI treat
 442 left and right-handed particles indistinctly in contrast to the former. Fortunately, the
 443 weak hypercharge, which is a combination of the weak isospin and the electric charge
 444 (eqn 2.2) is suitable to be used since it is conserved by the EI and WI. Thus, the
 445 symmetry group to be considered is

$$G \equiv SU(2)_L \otimes U(1)_Y \quad (2.4)$$

446 A detailed mathematical treatment of the theory can be found in the literature and
 447 here only the fundamental results will be presented [22–25]. In the following, the uni-
 448 fied weak and electromagnetic interaction will be referred as “Electroweak Interaction
 449 (EWI)”. Consider the first generation of leptons⁸

$$\psi_1 = \begin{pmatrix} \nu_e \\ e^- \end{pmatrix}_L, \quad \psi_2 = \nu_{eR}, \quad \psi_3 = e_R^- \quad (2.5)$$

450 The charged fermionic currents are given by:

$$J_\mu \equiv J_\mu^+ = \bar{\nu}_{eL} \gamma_\mu e_L, \quad J_\mu^\dagger \equiv J_\mu^- = \bar{e}_L \gamma_\mu \nu_L \quad (2.6)$$

451 and the free lagrangian is given by

$$\mathcal{L}_0 = \sum_{j=1}^3 i \bar{\psi}_j(x) \gamma^\mu \partial_\mu \psi_j(x) \quad (2.7)$$

452 Mass terms are included directly in the QED and QCD free lagrangians since they
 453 preserve the invariance under the symmetries transformations involved which treat
 454 left and right-handed similarly, however mass terms of the form

⁸ the treatment applies to any of the generations of fermions

$$m_W^2 W_\mu^\dagger(x) W^\mu(x) + \frac{1}{2} m_Z^2 Z_\mu(x) Z^\mu(x) - m_e \bar{\psi}_e(x) \psi_e(x) \quad (2.8)$$

which represent the mass of W^\pm , Z and electrons, are not invariant under G transformations, therefore the gauge fields described by the EWI are in principle massless. It is clear that the gauge fields are not massless, however, they have to acquire mass through a mechanism compatible with the gauge invariance; that mechanism is known as the “Higgs mechanism” and will be considered later in this section. The global transformations in the combined symmetry group G are given by

$$\begin{aligned} \psi_1(x) &\xrightarrow{G} \psi'_1(x) \equiv U_Y U_L \psi_1(x), \\ \psi_2(x) &\xrightarrow{G} \psi'_2(x) \equiv U_Y \psi_2(x), \\ \psi_3(x) &\xrightarrow{G} \psi'_3(x) \equiv U_Y \psi_3(x) \end{aligned} \quad (2.9)$$

where U_L represent the $SU(2)_L$ transformation acting on the weak isospin doublet only and U_Y represent the $U(1)_Y$ transformation acting on all the weak isospin multiplets. They are given by:

$$U_L \equiv \exp\left(i \frac{\sigma_i}{2} \alpha^i\right), \quad U_Y \equiv \exp(i y_i \beta) \quad (i = 1, 2, 3) \quad (2.10)$$

with σ_i the Pauli matrices and y_i the weak hypercharges. In order to promote the transformations from global to local keeping the invariance, it is required that $\alpha^i = \alpha^i(x)$ and $\beta = \beta(x)$ and the replace of the ordinary derivatives by the covariant derivatives:

$$\begin{aligned}
D_\mu \psi_1(x) &\equiv \left[\partial_\mu + ig\sigma_i W_\mu^i(x)/2 + ig'y_1 B_\mu(x) \right] \psi_1(x) \\
D_\mu \psi_2(x) &\equiv \left[\partial_\mu + ig'y_2 B_\mu(x) \right] \psi_2(x) \\
D_\mu \psi_3(x) &\equiv \left[\partial_\mu + ig'y_3 B_\mu(x) \right] \psi_3(x)
\end{aligned} \tag{2.11}$$

468 introducing four gauge fields, $W_\mu^i(x)$ and $B_\mu(x)$, in the process. The covariant deriva-
469 tives (eqn 2.11) are required to transform in the same way as fermion fields $\psi_i(x)$
470 themselves, therefore, the gauge fields transform as:

$$\begin{aligned}
B_\mu(x) &\xrightarrow{G} B'_\mu(x) \equiv B_\mu(x) - \frac{1}{g'} \partial_\mu \beta(x) \\
W_\mu^i(x) &\xrightarrow{G} W_\mu^{i\prime}(x) \equiv W_\mu^i(x) - \frac{i}{g} \partial_\mu \alpha_i(x) - \varepsilon_{ijk} \alpha_i(x) W_\mu^j(x)
\end{aligned} \tag{2.12}$$

471 The G invariant version of the lagrangian density 2.7 can be written as:

$$\mathcal{L}_0 = \sum_{j=1}^3 i\bar{\psi}_j(x) \gamma^\mu D_\mu \psi_j(x) \tag{2.13}$$

472 where free massless fermion and gauge fields and fermion-gauge boson interactions
473 are included. EWI lagrangian density must additionally include kinetic terms for the
474 gauge fields (\mathcal{L}_G) which are built from the field strengths, according to:

$$B_{\mu\nu}(x) \equiv \partial_\mu B_\nu - \partial_\nu B_\mu \tag{2.14}$$

$$W_{\mu\nu}^i(x) \equiv \partial_\mu W_\nu^i(x) - \partial_\nu W_\mu^i(x) - g\varepsilon^{ijk} W_\mu^j W_\nu^k \tag{2.15}$$

475 last term in eqn. 2.15 is added in order to hold the gauge invariance, therefore

$$\mathcal{L}_G = -\frac{1}{4}B_{\mu\nu}(x)B^{\mu\nu}(x) - \frac{1}{4}W_{\mu\nu}^i(x)W_i^{\mu\nu}(x) \quad (2.16)$$

476 which contains not only the free gauge fields contributions but also the gauge fields
 477 self-interactions and interactions among them.

478 The three weak isospin conserved currents resulting from the $SU(2)_L$ symmetry are
 479 given by

$$J_\mu^i(x) = \frac{1}{2}\bar{\psi}_1(x)\gamma_\mu\sigma_i\psi_1(x) \quad (2.17)$$

480 while the weak hypercharge conserved current resulting from the $U(1)_Y$ symmetry is
 481 given by;

$$J_\mu^Y = \sum_{j=1}^3 \bar{\psi}_j(x)\gamma_\mu y_j\psi_j(x) \quad (2.18)$$

482 In order to evaluate the electroweak interactions modeled by an isotriplet fields W_μ^i
 483 which couples to isospin currents J_μ^i with strength g and additionally the singlet
 484 field B_μ which couples to the weak hypercharge current J_μ^Y with strength $g'/2$, the
 485 interaction lagrangian density to be considered is given by:

$$\mathcal{L}_I = -g J^{i\mu}(x) W_\mu^i(x) - \frac{g'}{2} J^Y\mu(x) B_\mu(x) \quad (2.19)$$

486 written in terms of the physical fields W_μ^\pm , Z_μ and A_μ .

487 Note that the weak isospin currents are not the same as the charged fermionic currents
 488 that were used to describe the WI (eqn2.6), since the weak isospin eigenstates are not
 489 the same as the mass eigenstates, but they are closely related

$$J_\mu = \frac{1}{2}(J_\mu^1 + iJ_\mu^2), \quad J_\mu^\dagger = \frac{1}{2}(J_\mu^1 - iJ_\mu^2) \quad (2.20)$$

490 The same happen with the gauge fields W_μ^i which are related to the mass eigenstates
 491 W^\pm by

$$W_\mu^+ = \frac{1}{\sqrt{2}}(W_\mu^1 - iW_\mu^2), \quad W_\mu^- = \frac{1}{\sqrt{2}}(W_\mu^1 + iW_\mu^2) \quad (2.21)$$

492 The fact that there are three weak isospin conserved currents was an indication that
 493 additionally to the charged fermionic currents which couples charged to neutral lep-
 494 tons there should be a neutral fermionic current that couples neutral fermions or
 495 electrically charged fermions that has the same electric charge and thus does not
 496 imply electric charge change. The third weak isospin current contains a term that
 497 is similar to the electromagnetic current (j_μ^{em}), indicating that there is a relation
 498 between them and resembling the Gell-Mann-Nishijima formula 2.2 adapted to elec-
 499 troweak interactions

$$Q = T_3 + \frac{Y_W}{2} \quad (2.22)$$

500 The same way as Q generates the $U(1)_{em}$ symmetry, the weak hypercharge generates
 501 the $U(1)_Y$ symmetry as said before. It is possible to write the relationship in terms
 502 of the currents as:

$$j_\mu^{em} = J_\mu^3 + \frac{1}{2}J_\mu^Y \quad (2.23)$$

503 The neutral gauge fields W_μ^3 and B_μ cannot be directly identified with the Z and the
 504 photon fields since the photon interacts similarly with left and right-handed fermions,
 505 however they are related through a linear combination give by:

$$A_\mu = B_\mu \cos\theta_W + W_\mu^3 \sin\theta_W \quad (2.24)$$

$$Z_\mu = -B_\mu \sin\theta_W + W_\mu^3 \cos\theta_W$$

506 where θ_W is known as the “Weinberg angle”. The interaction lagrangian is now given
 507 by

$$\mathcal{L}_I = -\frac{g}{\sqrt{2}}(J^\mu W_\mu^+ + J^{\mu\dagger} W_\mu^-) - \left(g \sin\theta_W J_\mu^3 + g' \cos\theta_W \frac{J_\mu^Y}{2}\right) A^\mu - \left(g \cos\theta_W J_\mu^3 - g' \sin\theta_W \frac{J_\mu^Y}{2}\right) Z^\mu \quad (2.25)$$

508 the first term is the weak charged current interaction, while the second term is the
 509 electromagnetic interaction under the condition

$$g \sin\theta_W = g' \cos\theta_W = e, \quad \frac{g'}{g} = \tan\theta_W \quad (2.26)$$

510 contained in the eqn.2.23; the third term is the neutral weak current.

511 Note that the neutral fields transformation given by the eqn. 2.24 can be written in
 512 terms of the coupling constants g and g' as:

$$A_\mu = \frac{g' W_\mu^3 + g B_\mu}{\sqrt{g^2 + g'^2}}, \quad Z_\mu = \frac{g W_\mu^3 - g' B_\mu}{\sqrt{g^2 + g'^2}} \quad (2.27)$$

513 So far, the lagrangian density describing the non-massive EWI is:

$$\mathcal{L}_{nmEWI} = \mathcal{L}_0 + \mathcal{L}_G \quad (2.28)$$

514 where fermion and gauge fields have been considered massless because their regular
 515 mass terms are manifestly non invariant under G transformations; therefore, masses
 516 have to be generated in a gauge invariant way. The mechanism by which this goal is

517 achieved is known as the “Higgs mechanism” and is closely connected to the concept
 518 of “spontaneous symmetry breaking”.

519 Spontaneous symmetry breaking

520 Figure 2.6 left shows a steel nail (top) which is subject to an external force; the form
 521 of the potential energy is also shown (bottom). Before reaching the critical force
 522 value, the system has rotational symmetry with respect to the nail axis; however,
 523 after the critical force value is reached the nail buckles (top right). The form of the
 524 potential energy (bottom right) changes preserving its rotational symmetry although
 525 its minimum does not exhibit that rotational symmetry any longer. Right before
 526 the nail buckles there is no indication of the direction the nail will bend because
 527 any of the directions is equivalent, but once the nail bends, choosing a direction, an
 528 arbitrary minimal energy state (ground state) is selected and it does not share the
 529 system rotational symmetry. This mechanism for reaching an asymmetric ground state
 530 is known as "*spontaneous symmetry breaking (SSB)*"

531 The way to introduce the SSB mechanism is adding the appropriate potential to the
 532 lagrangian:

$$\mathcal{L} = (\partial_\mu \phi)^\dagger (\partial^\mu \phi) - V(\phi), \quad V(\phi) = \mu^2 \phi^\dagger \phi + \lambda (\phi^\dagger \phi)^2 \quad (2.29)$$

533 Figure 2.7 shows a plot of the potential $V(\phi)$ in the case of a scalar field ϕ . If $\mu^2 > 0$
 534 the potential has only one minimum at $\phi = 0$ and describes a scalar field with mass μ . If
 535 $\mu^2 < 0$ the potential has a local maximum at $\phi = 0$ and two minima at $\phi = \pm \sqrt{-\mu^2/\lambda}$
 536 which enables the SSB mechanism to work.

537 In the case of a complex scalar field $\phi(x)$ the lagrangian (invariant under global $U(1)$)

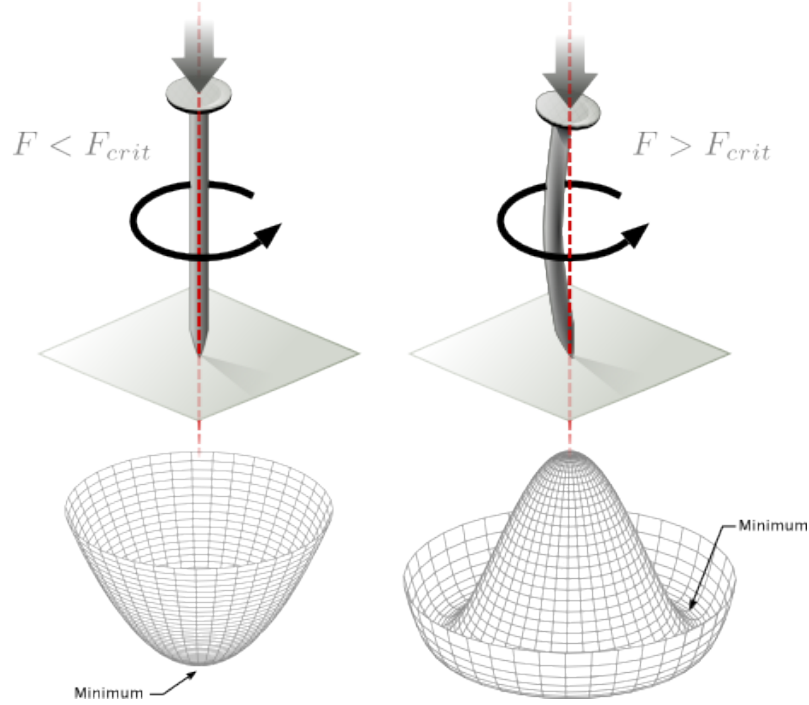


Figure 2.6: Spontaneous symmetry breaking mechanism. The steel nail, subject to an external force (top left), has rotational symmetry with respect to its axis. When the external force overcome a critical value the nail buckles (top right) choosing a minimal energy state (ground state) and “*spontaneously breaking the rotational symmetry*”. The potential energy (bottom) change but hold the rotational symmetry; however an infinite number of asymmetric ground states are generated and circularly distributed in the bottom of the potential [26].

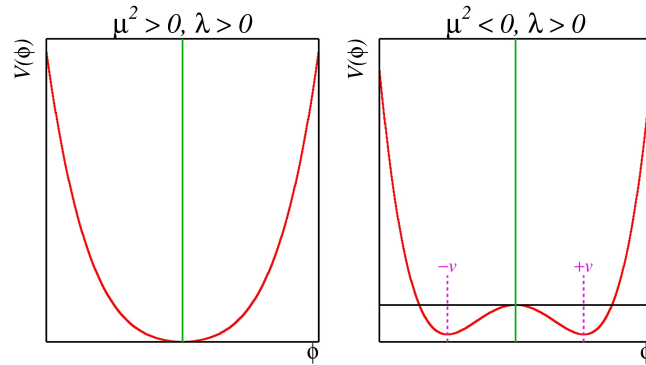


Figure 2.7: Shape of the potential $V(\phi)$ for $\lambda > 0$ and: $\mu^2 > 0$ (left) and $\mu^2 < 0$ (right). The case $\mu^2 < 0$ correspond to the potential suitable to introduce the SSB mechanism by choosing one of the two ground states which are connected via reflexion symmetry. [27].

538 transformations) and the potential are the same as 2.29, but the field is given by:

$$\phi(x) = \frac{1}{\sqrt{2}}(\phi_1 + i\phi_2) \quad (2.30)$$

539 As seen in figure 2.8, the potential has now an infinite number of minima circularly
 540 distributed along the ξ -direction which makes possible the occurrence of the SSB by
 541 choosing an arbitrary ground state, for instance $\xi = 0$ i.e. $\phi_1 = v, \phi_2 = 0$:

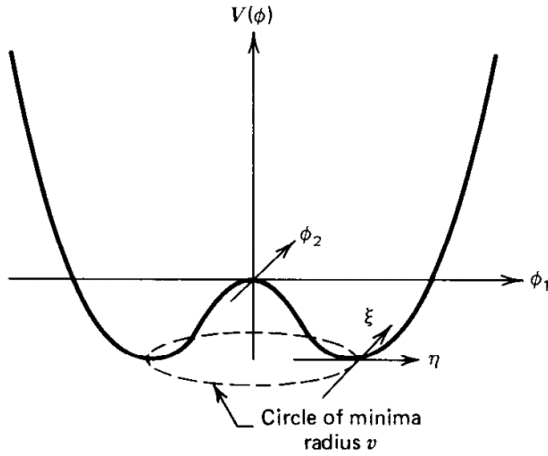


Figure 2.8: Potential for complex scalar field. There is a circle of minima of radius v along the ξ -direction [24].

$$\phi_0 = \frac{v}{\sqrt{2}} \exp(i\xi) \xrightarrow{\text{SSB}} \phi_0 = \frac{v}{\sqrt{2}} \quad (2.31)$$

542 As usual, excitations over the ground state are studied by making an expansion about
 543 it; thus, the excitation can be parametrized as:

$$\phi(x) = \frac{1}{\sqrt{2}}(v + \eta(x) + i\xi(x)) \quad (2.32)$$

544 which replaced in 2.29 produce a lagrangian in terms of the new fields η and ξ :

$$\mathcal{L}' = \frac{1}{2}(\partial_\mu \xi)^2 + \frac{1}{2}(\partial_\mu \eta)^2 + \mu^2 \eta^2 - V(\phi_0) - \lambda v \eta (\eta^2 + \xi^2) - \frac{\lambda}{4}(\eta^2 + \xi^2)^2 \quad (2.33)$$

545 where the last two terms represent the interactions and self-interaction between the
 546 two fields η and ξ . The particular feature of the SSB mechanism is revealed when
 547 looking to the first three terms of \mathcal{L}' . Before the SSB, only the massless ϕ field is
 548 present in the system; after the SSB there are two fields of which the η -field has
 549 acquired mass $m_\eta = \sqrt{-2\mu^2}$ while the ξ -field is still massless (see Figure 2.9)

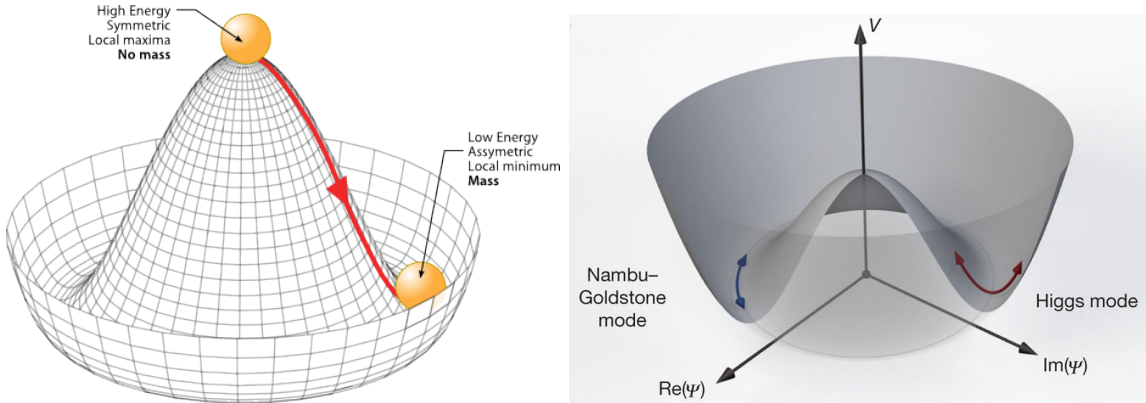


Figure 2.9: SSB mechanism for a complex scalar field [26].

550 Thus, the SSB mechanism arises as a method to generate mass but as a side effect a
 551 massless field is introduced in the system. This fact is known as the Goldstone theorem
 552 and states that a massless scalar field appears in the system for each continuous
 553 symmetry spontaneously broken. Another view of the Goldstone theorem states that
 554 a “if lagrangian is invariant under a continuous symmetry group G , but the vacuum
 555 is only invariant under a subgroup $H \subset G$, then there must exist as many massless
 556 spin-0 particles (Nambu-Goldstone bosons) as broken generators”. [25] The Nambu-
 557 Goldstone boson can be understood considering that the potential in the ξ -direction
 558 is flat so excitations in that direction are not energy consuming and then represent a

559 massless state.

560 Higgs mechanism

561 When the SSB mechanism is introduced in the formulation of the EWI in an attempt
 562 to generate the mass of the so far massless gauge bosons and fermions, an interesting
 563 effect is revealed. In order to keep the G symmetry group invariance and generate
 564 the mass of the EW gauge bosons a G invariant lagrangian density (\mathcal{L}_S) has to be
 565 added to the non massive EWI lagrangian (eqn. 2.28)

$$\mathcal{L}_S = (D_\mu \phi)^\dagger (D^\mu \phi) - \mu^2 \phi^\dagger \phi - \lambda (\phi^\dagger \phi)^2, \quad \lambda > 0, \mu^2 < 0 \quad (2.34)$$

$$D_\mu \phi = \left(i\partial_\mu - g \frac{\sigma_i}{2} W_\mu^i - g' \frac{Y}{2} B_\mu \right) \phi \quad (2.35)$$

566 ϕ has to be an isospin doublet of complex scalar fields so it preserve the G invariance;
 567 thus ϕ can be defined as:

$$\phi = \begin{pmatrix} \phi^+ \\ \phi^0 \end{pmatrix} \equiv \frac{1}{\sqrt{2}} \begin{pmatrix} \phi_1 + i\phi_2 \\ \phi_3 + i\phi_4 \end{pmatrix} \quad (2.36)$$

568 The minima of the potential are defined by;

$$\phi^\dagger \phi = \frac{1}{2} (\phi_1^2 + \phi_2^2 + \phi_3^2 + \phi_4^2) = -\frac{\mu^2}{2\lambda} \quad (2.37)$$

569 The choice of the ground state is critical. By choosing a ground state, invariant under
 570 $U(1)_{em}$ gauge symmetry, the photon will remain massless and the W^\pm and Z bosons
 571 masses will be generated which is exactly what is expected. In that sense, the best
 572 choice correspond to a weak isospin doublet with $T_3 = -1/2$, $Y_W = 1$ and $Q = 0$ which
 573 define a ground state with $\phi_1 = \phi_2 = \phi_4$ and $\phi_3 = v$:

$$\phi_0 \equiv \frac{1}{\sqrt{2}} \begin{pmatrix} 0 \\ v \end{pmatrix}, \quad v^2 \equiv -\frac{\mu^2}{\lambda} \quad (2.38)$$

574 The G symmetry has been broken and three Nambu-Goldstone bosons will appears.

575 The next step is to expand ϕ about the chosen ground state as:

$$\phi(x) = \frac{1}{\sqrt{2}} \exp\left(\frac{i}{v} \sigma_i \theta^i(x)\right) \begin{pmatrix} 0 \\ v + H(x) \end{pmatrix} \approx \frac{1}{\sqrt{2}} \begin{pmatrix} \theta_1(x) + i\theta_2(x) \\ v + H(x) - i\theta_3(x) \end{pmatrix} \quad (2.39)$$

576 to describe fluctuations from the ground state ϕ_0 . The fields $\theta_i(x)$ represent the
 577 Nambu-Goldstone bosons while $H(x)$ is known as “higgs field”. The fundamental
 578 feature of the parametrization used is that the dependence on the $\theta_i(x)$ fields is
 579 factored out in a global phase that can be eliminated by taking the physical “unitary
 580 gauge” $\theta_i(x) = 0$. Therefore the expansion about the ground state is given by:

$$\phi(x) \frac{1}{\sqrt{2}} \begin{pmatrix} 0 \\ v + H(x) \end{pmatrix} \quad (2.40)$$

581 which replaced in \mathcal{L}_S (eqn 2.34) result in a lagrangian containing the now massive
 582 three gauge bosons W^\pm, Z , one massless gauge boson (photon) and the new higgs field
 583 (H). The three degrees of freedom corresponding to the Nambu-goldstone bosons are
 584 now integrated into the massive gauge bosons as their longitudinal polarizations which
 585 were not available when they were massless particles. The effect by which vector boson
 586 fields acquire mass after an spontaneous symmetry breaking but without an explicit
 587 gauge invariance breaking is known as the “*Higgs mechanism*”.

588 The mechanism was proposed by three independent groups: F.Englert and R.Brout
 589 in August 1964 [28]; P.higgs in October 1964 [29]; and G.Guralnik, C.Hagen and
 590 T.Kibble in November 1964 [30]; however its importance was not realized until S.Glashow
 591 [8], A.Salam [9] and S.Weinberg [10] independently proposed that electromagnetic and

592 weak interactions are two manifestations of a more general interaction called “elec-
 593 troweak interaction” in 1967.

594 Masses of the gauge bosons

595 The mass of the gauge bosons is extracted by evaluating the kinetic part of lagrangian
 596 \mathcal{L}_S in the ground state⁹, i.e.

$$\left| \left(\partial_\mu - ig \frac{\sigma_i}{2} W_\mu^i - i \frac{g'}{2} B_\mu \right) \phi_0 \right|^2 = \left(\frac{1}{2} v g \right)^2 W_\mu^+ W^{-\mu} + \frac{1}{8} v^2 (W_\mu^3, B_\mu) \begin{pmatrix} g^2 & -gg' \\ -gg' & g'^2 \end{pmatrix} \begin{pmatrix} W^{3\mu} \\ B^\mu \end{pmatrix} \quad (2.41)$$

597 comparing with the typical mass term for a charged boson $M_W^2 W^+ W^-$:

$$M_W = \frac{1}{2} v g \quad (2.42)$$

The second term in the right side of the eqn.2.41 enclose the masses of the neutral bosons, but it needs to be written in terms of the gauge fields Z_μ and A_μ in order to be compared to the typical mass terms for neutral bosons, therefore using eqn. 2.27

$$\begin{aligned} \frac{1}{8} v^2 [g^2 (W_\mu^3)^2 - 2gg' W_\mu^3 B^\mu + g'^2 B_\mu^2] &= \frac{1}{8} v^2 [g W_\mu^3 - g' B_\mu]^2 + 0[g' W_\mu^3 + g B_\mu]^2 \quad (2.43) \\ &= \frac{1}{8} v^2 [\sqrt{g^2 + g'^2} Z_\mu]^2 + 0[\sqrt{g^2 + g'^2} A_\mu]^2 \end{aligned}$$

598 and then

$$M_Z = \frac{1}{2} v \sqrt{g^2 + g'^2}, \quad M_A = 0 \quad (2.44)$$

⁹ known also as the vacuum expectation value

599 **Masses of the fermions**

600 The lepton mass terms can be generated by introducing a gauge invariant lagrangian
 601 term describing the Yukawa coupling between the lepton field and the higgs field:

$$\mathcal{L}_{Yl} = -G_l \left[(\bar{\nu}_l, \bar{l})_L \begin{pmatrix} \phi^+ \\ \phi^0 \end{pmatrix} l_R + \bar{l}_R (\phi^-, \bar{\phi}^0) \begin{pmatrix} \nu_l \\ l \end{pmatrix}_L \right], \quad l = e, \mu, \tau \quad (2.45)$$

602 After the SSB and replacing the usual field expansion about the ground state (eqn.2.38)
 603 into \mathcal{L}_{Yl} , the mass term arise:

$$\mathcal{L}_{Yl} = -m_l (\bar{l}_L l_R + \bar{l}_R l_L) - \frac{m_l}{v} (\bar{l}_L l_R + \bar{l}_R l_L) H = -m_l \bar{l} l \left(1 + \frac{H}{v} \right) \quad (2.46)$$

604

$$m_l = \frac{G_l}{\sqrt{2}} v \quad (2.47)$$

605 the additional term represent the lepton-higgs interaction. The quark masses are
 606 generated in a similar way as lepton masses but for the upper member of the quark
 607 doublet a different higgs doublet is needed:

$$\phi_c = -i\sigma_2 \phi^* = \begin{pmatrix} -\bar{\phi}^0 \\ \phi^- \end{pmatrix} \quad (2.48)$$

608 Additionally, given that the quark isospin doublets are not constructed in terms of
 609 the mass eigenstates but in terms of the flavor eigenstates as shown in table2.5, the
 610 coupling parameters will be related to the CKM matrix elements; thus the quark
 611 lagrangian is given by:

$$\mathcal{L}_{Yq} = -G_d^{i,j} (\bar{u}_i, \bar{d}'_i)_L \begin{pmatrix} \phi^+ \\ \phi^0 \end{pmatrix} d_{jR} - G_u^{i,j} (\bar{u}_i, \bar{d}''_i)_L \begin{pmatrix} -\bar{\phi}^0 \\ \phi^- \end{pmatrix} u_{jR} + h.c. \quad (2.49)$$

612 with $i,j=1,2,3$. After SSB and expansion about the ground state, tha diagonal form

613 of \mathcal{L}_{Yq} is:

$$\mathcal{L}_{Yq} = -m_d^i \bar{d}_i d_i \left(1 + \frac{H}{v}\right) - m_u^i \bar{u}_i u_i \left(1 + \frac{H}{v}\right) \quad (2.50)$$

614 Fermion masses depends on arbitrary couplings G_l and $G_{u,d}$ and are not predicted
615 by the theory.

616 The Higgs field

617 After the characterization of the fermions and gauge bosons as well as their interac-
618 tions, it is needed to characterize the higgs field itself. The lagrangian \mathcal{L}_S in eqn:2.34
619 written in terms of the gauge bosons is given by:

$$\mathcal{L}_S = \frac{1}{4} \lambda v^4 + \mathcal{L}_H + \mathcal{L}_{HV} \quad (2.51)$$

620

$$\mathcal{L}_H = \frac{1}{2} \partial_\mu H \partial^\mu H - \frac{1}{2} m_H^2 H^2 - \frac{1}{2v} m_H^2 H^3 - \frac{1}{8v^2} m_H^2 H^4 \quad (2.52)$$

621

$$\mathcal{L}_{HV} = m_H^2 W_\mu^+ W^{\mu-} \left(1 + \frac{2}{v} H + \frac{2}{v^2} H^2\right) + \frac{1}{2} m_Z^2 Z_\mu Z^\mu \left(1 + \frac{2}{v} H + \frac{2}{v^2} H^2\right) \quad (2.53)$$

Property	Value
Electric charge	0
Colour charge	0
Spin	0
Weak isospin	-1/2
Weak hypercharge	1
Parity	1
Mass GeV/c ²	$125.09 \pm 0.21 \text{ (stat.)} \pm 0.11 \text{ (syst.)}$

Table 2.6: Higgs boson properties.

622

623 The mass of the higgs boson is deduced as usual from the mass term in the
624 lagrangian resulting in:

$$m_H = \sqrt{-2\mu^2} = \sqrt{2\lambda}v \quad (2.54)$$

however it is not predicted either by the theory. The experimental efforts to find the higgs boson, carried out by the CMS and ATLAS experiments¹⁰, gave great results by July of 2012 when the discovery of a new particles was announced and which is compatible with the higgs boson predicted by the electroweak theory [31,32]. Although at that time there was a taste of reserve about to call the new particle “higgs boson” today is widely accepted this particle as the SM higgs boson. The measurement of the higgs mass has been reported by both experiments and the official value [33] is in table 2.6. The vacuum expectation value v is fixed by the Fermi coupling G_F according to $v = (\sqrt{2}G_F)^{1/2} \approx 246\text{GeV}$.

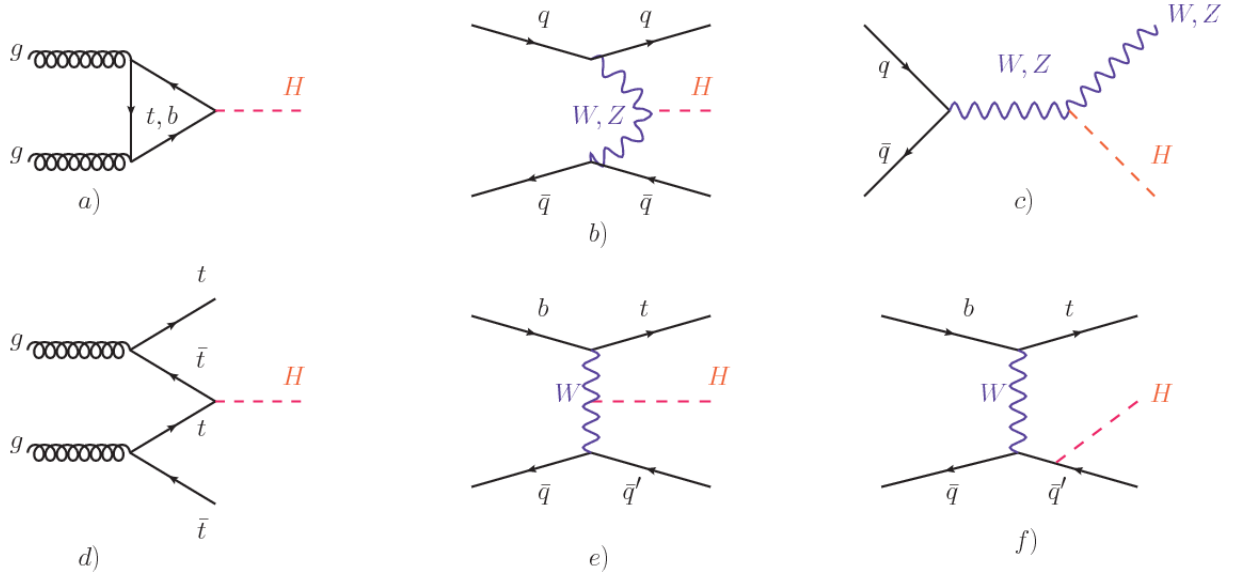


Figure 2.10: Main Higgs production mechanism Feynman diagrams. a) gluon-gluon fusion, b) vector boson fusion (VBF), c) Higgs-strahlung, d) Associated production with a top or bottom quark pair, e-f) associated production with a single top quark.

As shown in eqns 2.45,2.49 and 2.53, higgs-fermion interaction is proportional to the fermion mass while higgs-boson interaction is proportional to the square of the boson mass which imply that the higgs production and decay mechanisms are dominated by

¹⁰ CMS stands for Compact Muon Solenoid; ATLAS stand for A Toroidal LHC Apparatus. Both are general experiments held at the Large Hadron Collider(LHC)

637 couplings $H - (W, Z, t, b, \tau)$. Figure 2.10 shows the Feynman diagrams for the leading
 638 order higgs production processes while the cross section for higgs production as a
 639 function of the center of mass-energy (\sqrt{s}) for pp collisions is showed in the figure
 640 2.11 left. Table2.7 present the cross sections for $m_H = 125 GeV/c^2$.

$\sqrt{s}(\text{TeV})$	Production cross section (in pb) for $m_H = 125 GeV/c^2$					total
	ggF	VBF	WH	ZH	tH	
7	$16.9 \pm 5\%$	$1.24 \pm 2\%$	$0.58 \pm 3\%$	$0.34 \pm 4\%$	$0.09^{+8\%}_{-14\%}$	19.1
8	$21.4 \pm 5\%$	$1.60 \pm 2\%$	$0.70 \pm 3\%$	$0.42 \pm 5\%$	$0.13^{+8\%}_{-13\%}$	24.2
13	$48.6 \pm 5\%$	$3.78 \pm 2\%$	$1.37 \pm 2\%$	$0.88 \pm 5\%$	$0.50^{+9\%}_{-13\%}$	55.1
14	$54.7 \pm 5\%$	$4.28 \pm 2\%$	$1.51 \pm 2\%$	$0.99 \pm 5\%$	$0.60^{+9\%}_{-13\%}$	62.1

Table 2.7: The SM Higgs boson production cross sections for $m_H = 125 GeV/c^2$.in pp collisions as a function of the center of mass energy, \sqrt{s} . The predictions for the ggF channel at the LHC include the latest N3LO results leading to reduced theoretical uncertainties by a factor around 2 compared to the N2LO results. [35]

641

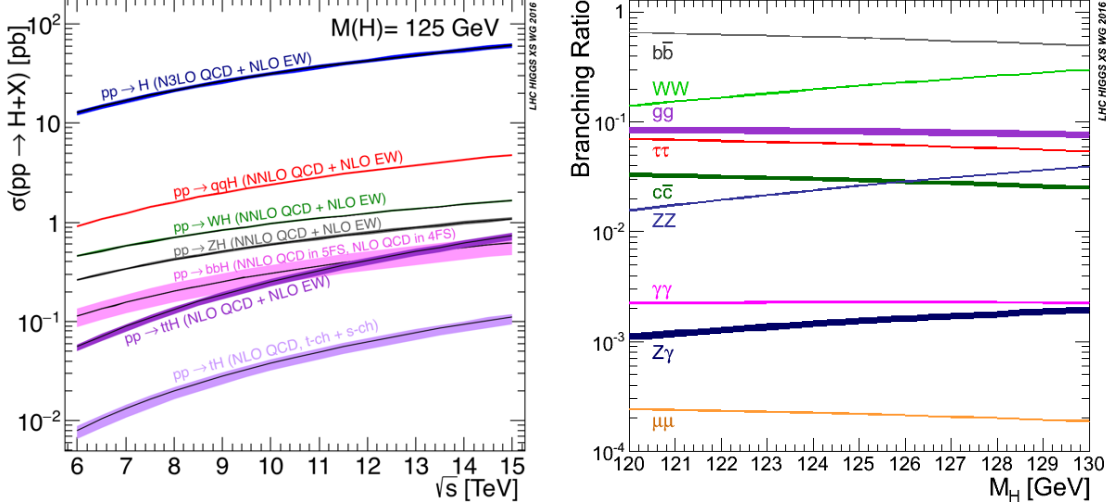


Figure 2.11: Higgs production cross sections (left) and decay branching ratios (right) for the main mechanisms. The VBF is indicated as qqH [34].

642 The main production mechanism is the gluon fusion ($pp \rightarrow H$). Since the higgs boson
 643 does not couples to gluons the mechanism proceed through the exchange of a virtual

644 top quark. Note that in this process the higgs boson is produced alone which makes
 645 this mechanism experimentally clean when combined with the two-photon or the
 646 four-lepton decay channels.

647 The vector boson fusion($pp \rightarrow qqH$) has the second largest production cross section.
 648 The scattering of two fermions is mediated by a vector boson which emits a higgs
 649 boson. The final state fermions tend to be located in the forward region of the detector
 650 which use to be used when analyzing the datasets.

651 In the higgs-strahlung ($pp \rightarrow WH, pp \rightarrow ZH$) two fermions annihilate to form a vector
 652 boson. If the initial fermions have enough energy the vector boson can eventually will
 653 emit a higgs boson. The associated production with a top or bottom quark pair and
 654 the associated production with a single top quark ($pp \rightarrow bbH, pp \rightarrow ttH, pp \rightarrow tH$)
 655 have less cross section than the main three mechanism above but they provide a good
 656 strategy to test the higgs-top coupling. Analysis reported in this thesis is developed
 657 using this production mechanism.

658 In regard to the decay channels, the branching ratios (BR) can be predicted with
 659 accuracy once the higgs mass is known. In the figure 2.11 right, a plot of the BR as
 660 a function of the higgs mass is presented. The largest BR correspond to the $b\bar{b}$ pair
 661 decay channel (see table 2.8); in this thesis the $H \rightarrow WW$ channel will be considered.

Decay channel	Branching ratio	Rel. uncertainty
$H \rightarrow \gamma\gamma$	2.27×10^{-3}	$+5.0\% - 4.9\%$
$H \rightarrow ZZ$	2.62×10^{-2}	$+4.3\% - 4.1\%$
$H \rightarrow W^+W^-$	2.14×10^{-1}	$+4.3\% - 4.2\%$
$H \rightarrow \tau^+\tau^-$	6.27×10^{-2}	$+5.7\% - 5.7\%$
$H \rightarrow b\bar{b}$	5.84×10^{-1}	$+3.2\% - 3.3\%$
$H \rightarrow Z\gamma$	1.53×10^{-3}	$+9.0\% - 8.9\%$
$H \rightarrow \mu^+\mu^-$	2.18×10^{-4}	$+6.0\% - 5.9\%$

Table 2.8: The branching ratios and the relative uncertainty for a SM Higgs boson with $m_H = 125 GeV/c^2$. [35]

662

⁶⁶³ The tHq process

⁶⁶⁴ The CP phase

665 Chapter 3

666 The CMS experiment at the LHC

667 Located in the Swiss-French border, the European Council for Nuclear Research
668 (CERN) is the largest scientific organization leading the particle physics research;
669 about 13000 people in a broad range of fields including users, students, scientist, en-
670 gineers among others, contribute to the data taking and analysis, with the goal of
671 unveil the secrets of the nature and reveal the fundamental structure of the universe.
672 CERN is also the home of the Large Hadron Collider (LHC), the largest circular
673 particle accelerator around the world, where protons (or heavy ions) traveling close
674 to the speed of light are made to collide together. These collisions open a window to
675 investigate how particles (and their constituents if they are composite) interact with
676 each other, providing clues about the laws of the nature.

677 LHC can run in three modes depending on the particles being accelerated:

- 678 • Proton-Proton collisions (pp) mostly general purpose experiments.
- 679 • Lead-Lead collisions (Pb-Pb) Heavy ion experiments.
- 680 • Proton-Lead collisions (p-Pb).

681 There are several accelerating stages before the injection to the LHC ring. In the
682 pp mode, after removing the electrons from Hydrogen atoms in a bottle, protons are
683 accelerated in the LINAC2 to 50MeV and then injected into the proton synchrotron
684 booster (BOOSTER) to reach 1.4 GeV in energy. The next boost is provided at the
685 proton synchrotron(PS) up to 26 GeV, followed by the injection to the super proton
686 synchrotron (SPS) where protons are accelerated to 450 GeV. Finally, protons are
687 injected in the LHC where they are accelerated to the target energy of 6.5 TeV. In
688 the Pb-Pb mode, the Lead ions are first accelerated in the LINAC3 and then passed as
689 long pulses to the Low energy ion ring (LEIR) to be converted into short and dense
690 bunches, each containing 7×10^7 lead ions. LEIR accelerate the bunches from 4.2
691 MeV to 72 MeV. The ions are then passed to the PS to follow the rest of acceleration
692 process up to 2.8TeV/n en the LHC ring. Figure 3.1 show an overview of the CERN
693 accelerating complex.

694 The LHC

695 The LHC is a 27 km ring composed by superconducting magnets and accelerating
696 structures (among other components) which boost the particles traveling inside it. It
697 is installed in the same tunnel where the large electron-positron (LEP) collider were
698 located, taking advantage of the existing infraestructure as shown in the figure 3.2.
699 Two particle beams travel counter-rotating in two separed beam pipes kept at ultra
700 high vacuum. In 2008, the first set of collisions involved protons with center-of-mass
701 energy of 7 TeV after which the energy was increased to 8 TeV in 2012 and to 13 TeV
702 in 2015.

703 In order to keep the protons in the circular trajectory carrying that amount of
704 energy, strong magnetic fields are needed, bringing the superconductivity into scene.

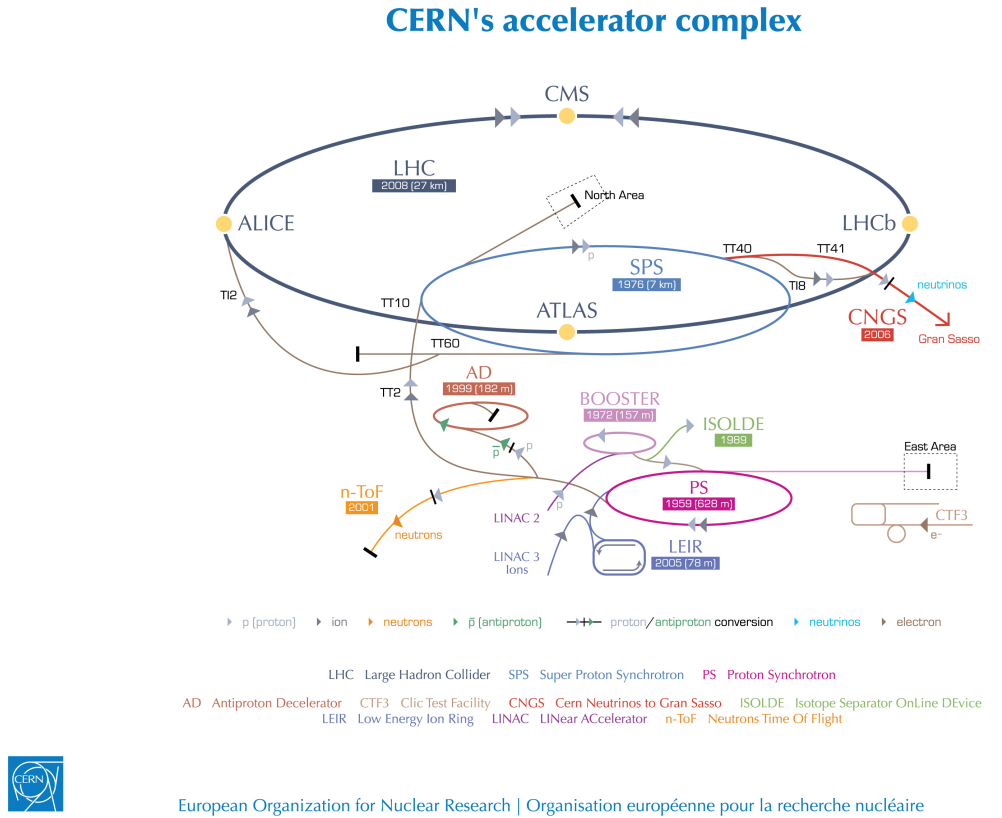
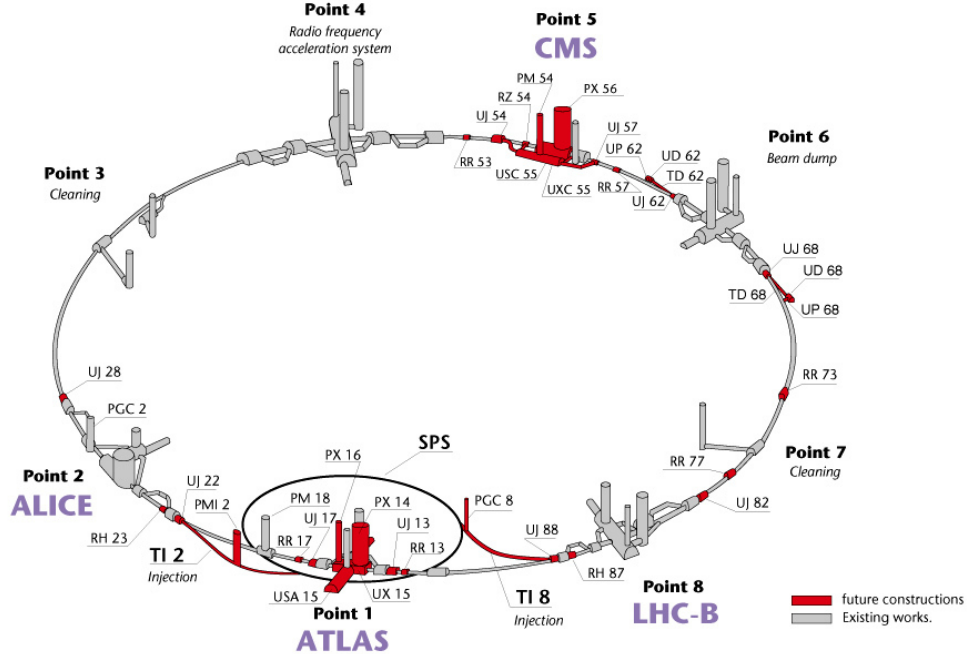


Figure 3.1: ref. C.Lefevre, “The CERN accelerator complex,” (2008). CERN-DI-0812015.

705 The superconducting dipole magnets used in LHC are made of a NbTi alloy, capable
 706 to transport currents of about $12000A$ when cooled at a temperature below $2K$ by
 707 using liquid helium; that current generates a magnetic fields of 8.3 T. Figure 3.3 show
 708 the transverse view of the LHC dipole magnets. Additionally, quadrupolar multipoles are used to correct
 709 effects generated by the interaction among protons in the beam as well as interactions
 710 within the beam pipe.

712 Regarding to the longitudinal acceleration of the protons, a system of 16 radio-
 713 frecuency cavities (RF) (8 per beam) is used; Inside the cavities, the electromagnetic
 714 waves become resonant transferring the maximum energy to the particle flight through
 715 it. Cavities are cooled at 4.5 K. On LHC the RF oscillation frecuency is $400MHz$ and

Layout of the LEP tunnel including future LHC infrastructures.



CERN AC _ hf238 _ V02/02/98

Figure 3.2: ref. J.-L. Caron , “Layout of the LEP tunnel including future LHC infrastructures.. L’ensemble du tunnel LEP avec les futures infrastructures LHC.”, <https://cds.cern.ch/record/841542> (Nov, 1993). AC Collection. Legacy of AC. Pictures from 1992 to 2002..

716 the protons are carefully timed so additionally to the acceleration effect the bunch
 717 structure of the beam is preserved. The Beam is made of 2808 “bunches” which are
 718 packages of 1.15×10^{11} protons ???. If LHC is at full energy, protons with the right
 719 energy does not feel any accelerating force but those with a different energy will be
 720 accelerated or decelerated to keep them in the bunch. The paths followed by particles
 721 during the acceleration process are shown in figure 3.1.

722 Once the beams reach the desired energy, they are brought to cross each other
 723 producing proton-proton collisions. The bunch crossing happens in precise places
 724 where the LHC experiments are located. As seen in figure 3.2, it was needed to

LHC DIPOLE : STANDARD CROSS-SECTION

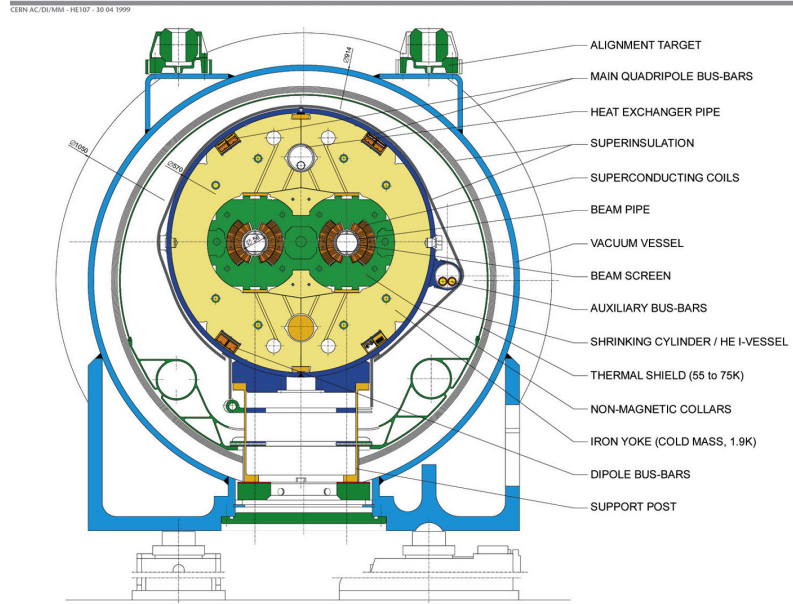


Figure 3.3: ref. ACTeam, “Diagram of an LHC dipole magnet. Schéma d’un aimant dipôle du LHC,” (1999). CERN-DI-9906025.

725 build the caverns for CMS and ATLAS as well as some additional facilities, but
 726 most of the initial LEP infrastructure has been used to allocate additional collision
 727 points. The highest luminosity is delivered at the CMS (point 5) and ATLAS (point
 728 1) experiments, which are general purpose experiments, enabled to explore physics
 729 in any of the collision modes. LHCb (point 8) experiment is optimized to explore
 730 B-physics, while ALICE (point 2) is optimized for heavy ion collisions researches;
 731 TOTEM (point 5) and LHCf (point 1) are dedicated to forward physics studies and
 732 MoEDAL (point 8) is intended for monopoles or massive pseudo stable particles
 733 studies.

734 The CMS experiment

735 The Compact Muon Solenoid (CMS) is a general purpose detector designed to conduct
 736 research in a wide range of physics from standard model to new physics like extra

737 dimensions and dark matter. Located at the point 5 in the LHC layout as shown in
 738 figure 3.2, CMS is composed by several detection systems distributed in a cylindrical
 739 structure where the main feature is a solenoid magnet made of superconducting cable
 740 capable to generate a 3.8 T magnetic field. In total, CMS weight about 14000 tons
 741 in a very compact 21.6 m long and 14.6 m diameter cylinder (include areference for
 742 CMS TDR). It was built in 15 separated sections at the ground level and lowered
 743 to the cavern individually to be assembled. Figure 3.4 show the layout of the CMS
 744 detector (CMS TDR).

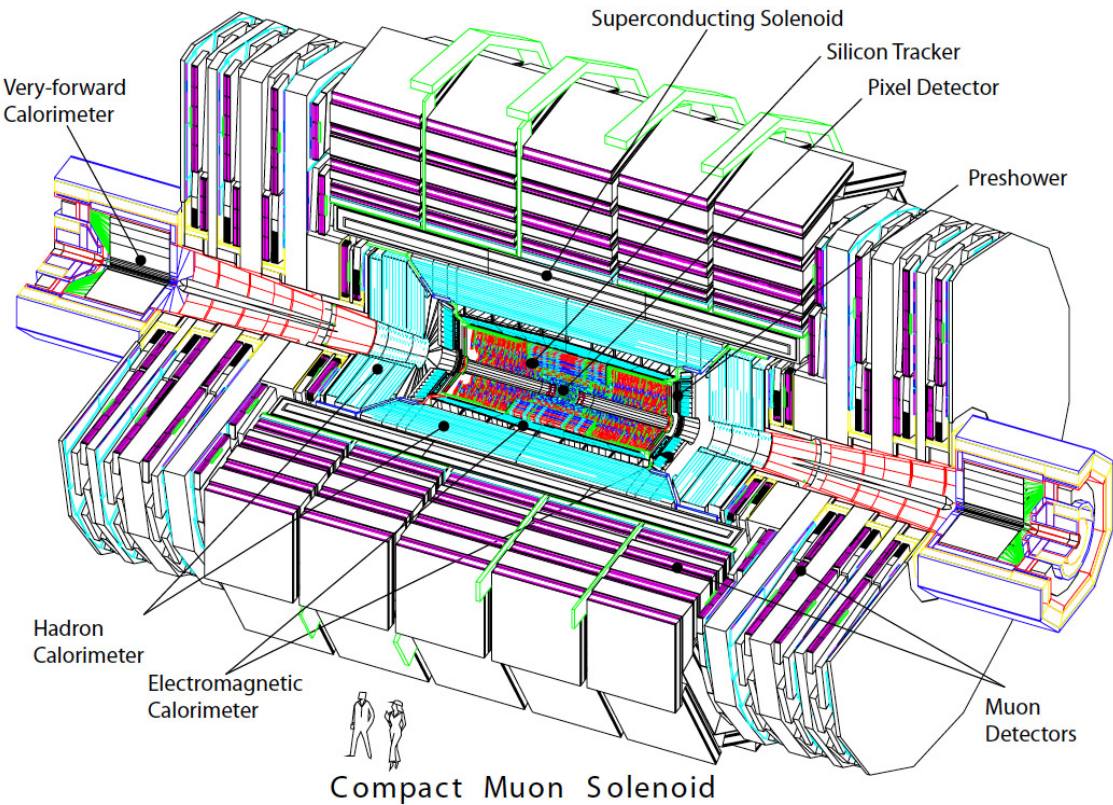


Figure 3.4: ref: CMS Collaboration, “Detector Drawings”, CMS-PHO-GEN-2012-002, <http://cds.cern.ch/record/1433717>, 2012.

745 Chapter 4

746 Search for production of a Higgs boson and 747 a single top quark in multilepton final states 748 in pp collisions at $\sqrt{s} = 13$ TeV

749 Introduction

750 This chapter present the search for the associated production of a Higgs boson and
 751 a single top quark events with three leptons in the final state, targeting Higgs decay
 752 modes to WW , ZZ , and $\tau\tau$. The analysis uses the 13 TeV dataset produced in 2016,
 753 corresponding to an integrated luminosity of 35.9fb^{-1} . It is based on and expands
 754 previous analyses at 8 TeV [36, 37] and searches for associated production of $t\bar{t}$ and
 755 Higgs in the same channel [38], and complements searches in other decay channels
 756 targeting $H \rightarrow b\bar{b}$ [39].

757 The production cross section of the single top plus Higgs boson (tHq) process
 758 is driven by a destructive interference of two main diagrams (see Fig. 4.1), where
 759 the Higgs couples to either the W boson or the top quark. Any deviation from the
 760 standard model (SM) in the Higgs coupling structure could therefore lead to a large

enhancement of the cross section, making this analysis sensitive to such deviations.
A second process, where the Higgs and top quark are accompanied by a W boson
(tHW) has similar behavior, albeit with a weaker interference pattern.

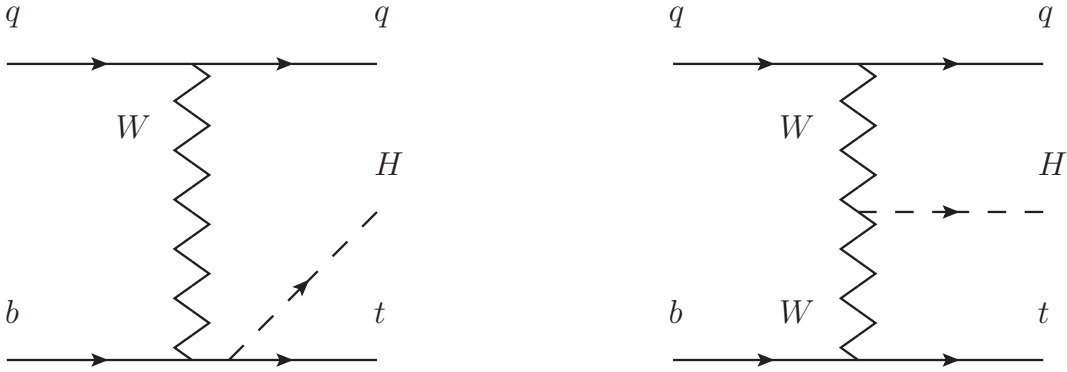


Figure 4.1: The two leading-order diagrams of tHq production.

We selects events with three leptons and a b tagged jet in the final state. The tHq signal contribution is then determined in a fit of the observed data to two multivariate classifier outputs, each trained to discriminate against one of the two dominant backgrounds of events with non-prompt leptons from $t\bar{t}$ and of associated production of $t\bar{t}$ and vector bosons ($t\bar{t}W$, $t\bar{t}Z$). The fit result is then used to set an upper limit on the combined $t\bar{t}H$, tHq and tHW production cross section, as a function of the relative coupling strengths of Higgs and top quark and Higgs and W boson, respectively.

771 Data and MC Samples

The data considered in this analysis were collected by the CMS experiment during 2016 and correspond to a total integrated luminosity of 35.9fb^{-1} . Only periods when the CMS magnet was on were considered when selecting the data samples, that corresponds to the 23 Sep 2016 (Run B to G) and PromptReco (Run H) versions

of the datasets. The MC samples used in this analysis correspond to the RunI-ISummer16MiniAODv2 campaign produced with CMSSW 80X. The two signal samples (for tHq and tHW) were produced with MG5_aMC@NLO (version 5.222), in leading-order order mode, and are normalized to next-to-leading-order cross sections, see Tab. 4.1. Each sample is generated with a set of event weights corresponding to different values of κ_t and κ_V couplings as shown in Tab. 4.2.

Full 2016 dataset and MC samples

Sample	σ [pb]	BF
/THQ_Hincl_13TeV-madgraph-pythia8_TuneCUETP8M1/	0.7927	0.324
/THW_Hincl_13TeV-madgraph-pythia8_TuneCUETP8M1/	0.1472	1.0

Table 4.1: Signal samples and their cross section and branching fraction used in this analysis. See Ref. [40] for more details.

Different MC generators were used to generate the background processes. The dominant sources ($t\bar{t}$, $t\bar{t}W$, $t\bar{t}Z$, $t\bar{t}H$) were produced using AMC@NLO interfaced to PYTHIA8, and are scaled to NLO cross sections. Other processes are simulated using POWHEG interfaced to PYTHIA, or bare PYTHIA (see table 4.3 and [38] for more details).

Triggers

We consider online-reconstructed events triggered by one, two, or three leptons. Single-lepton triggers are included to boost the acceptance of events where the p_T of the sub-leading lepton falls below the threshold of the double-lepton triggers. Additionally, by including double-lepton triggers in the ≥ 3 lepton category, as well as single-lepton triggers in all categories, we increase the efficiency, considering the logical “or” of the trigger decisions of all the individual triggers in a given category.

		tHq			tHW		
κ_V	κ_t	sum of weights	cross section [pb]	sum of weights	cross section [pb]	LHE weights	
1.0	-3.0	35.700022	2.991	11.030445	0.6409	LHEweight_wgt[446]	
1.0	-2.0	20.124298	1.706	5.967205	0.3458	LHEweight_wgt[447]	
1.0	-1.5	14.043198	1.205	4.029093	0.2353	LHEweight_wgt[448]	
1.0	-1.25	11.429338	0.9869	3.208415	0.1876	LHEweight_wgt[449]	
1.0	-1.0		0.7927		0.1472		
1.0	-0.75	7.054998	0.6212	1.863811	0.1102	LHEweight_wgt[450]	
1.0	-0.5	5.294518	0.4723	1.339886	0.07979	LHEweight_wgt[451]	
1.0	-0.25	3.818499	0.3505	0.914880	0.05518	LHEweight_wgt[452]	
1.0	0.0	2.627360	0.2482	0.588902	0.03881	LHEweight_wgt[453]	
1.0	0.25	1.719841	0.1694	0.361621	0.02226	LHEweight_wgt[454]	
1.0	0.5	1.097202	0.1133	0.233368	0.01444	LHEweight_wgt[455]	
1.0	0.75	0.759024	0.08059	0.204034	0.01222	LHEweight_wgt[456]	
1.0	1.0	0.705305	0.07096	0.273617	0.01561	LHEweight_wgt[457]	
1.0	1.25	0.936047	0.0839	0.442119	0.02481	LHEweight_wgt[458]	
1.0	1.5	1.451249	0.1199	0.709538	0.03935	LHEweight_wgt[459]	
1.0	2.0	3.335034	0.2602	1.541132	0.08605	LHEweight_wgt[460]	
1.0	3.0	10.516125	0.8210	4.391335	0.2465	LHEweight_wgt[461]	
<hr/>							
1.5	-3.0	45.281492	3.845	13.426212	0.7825	LHEweight_wgt[462]	
1.5	-2.0	27.606715	2.371	7.809713	0.4574	LHEweight_wgt[463]	
1.5	-1.5	20.476088	1.784	5.594971	0.3290	LHEweight_wgt[464]	
1.5	-1.25	17.337465	1.518	4.635978	0.2749	LHEweight_wgt[465]	
1.5	-1.0	14.483302	1.287	3.775902	0.2244	LHEweight_wgt[466]	
1.5	-0.75	11.913599	1.067	3.014744	0.1799	LHEweight_wgt[467]	
1.5	-0.5	9.628357	0.874	2.352505	0.1410	LHEweight_wgt[468]	
1.5	-0.25	7.627574	0.702	1.789184	0.1081	LHEweight_wgt[469]	
1.5	0.0	5.911882	0.5577	1.324946	0.08056	LHEweight_wgt[470]	
1.5	0.25	4.479390	0.4365	0.959295	0.05893	LHEweight_wgt[471]	
1.5	0.5	3.331988	0.3343	0.692727	0.04277	LHEweight_wgt[472]	
1.5	0.75	2.469046	0.2558	0.525078	0.03263	LHEweight_wgt[473]	
1.5	1.0	1.890565	0.2003	0.456347	0.02768	LHEweight_wgt[474]	
1.5	1.25	1.596544	0.1689	0.486534	0.02864	LHEweight_wgt[475]	
1.5	1.5	1.586983	0.1594	0.615638	0.03509	LHEweight_wgt[476]	
1.5	2.0	2.421241	0.2105	1.170602	0.06515	LHEweight_wgt[477]	
1.5	3.0	7.503280	0.5889	3.467546	0.1930	LHEweight_wgt[478]	
<hr/>							
0.5	-3.0	27.432685	2.260	8.929074	0.5136	LHEweight_wgt[479]	
0.5	-2.0	13.956013	1.160	4.419093	0.2547	LHEweight_wgt[480]	
0.5	-1.5	8.924438	0.7478	2.757611	0.1591	LHEweight_wgt[481]	
0.5	-1.25	6.835341	0.5726	2.075247	0.1204	LHEweight_wgt[482]	
0.5	-1.0	5.030704	0.4273	1.491801	0.08696	LHEweight_wgt[483]	
0.5	-0.75	3.510528	0.2999	1.007273	0.05885	LHEweight_wgt[484]	
0.5	-0.5	2.274811	0.1982	0.621663	0.03658	LHEweight_wgt[485]	
0.5	-0.25	1.323555	0.1189	0.334972	0.01996	LHEweight_wgt[486]	
0.5	0.0	0.656969	0.06223	0.147253	0.008986	LHEweight_wgt[487]	
0.5	0.25	0.274423	0.02830	0.058342	0.003608	LHEweight_wgt[488]	
0.5	0.5	0.176548	0.01778	0.068404	0.003902	LHEweight_wgt[489]	
0.5	0.75	0.363132	0.03008	0.177385	0.009854	LHEweight_wgt[490]	
0.5	1.0	0.834177	0.06550	0.385283	0.02145	LHEweight_wgt[491]	
0.5	1.25	1.589682	0.1241	0.692099	0.03848	LHEweight_wgt[492]	
0.5	1.5	2.629647	0.2047	1.097834	0.06136	LHEweight_wgt[493]	
0.5	2.0	5.562958	0.4358	2.206057	0.1246	LHEweight_wgt[494]	
0.5	3.0	14.843102	1.177	5.609519	0.3172	LHEweight_wgt[495]	

Table 4.2: κ_V and κ_t combinations generated for the two signal samples and their NLO cross sections. The tHq cross section is multiplied by the branching fraction of the enforced leptonic decay of the top quark (0.324). See also Ref. [40].

Sample	σ [pb]
TTWJetsToLNu_TuneCUETP8M1_13TeV-amcatnloFXFX-madspin-pythia8	0.2043
TTZToLLNuNu_M-10_TuneCUETP8M1_13TeV-amcatnlo-pythia8	0.2529
ttHJetToNonbb_M125_13TeV_amcatnloFXFX_madspin_pythia8_mWCutfix /store/cmst3/group/susy/gpetrucc/13TeV/u/TTLL_m1to10_LO_NoMS_for76X/	0.2151 0.0283
WGToLNuG_TuneCUETP8M1_13TeV-madgraphMLM-pythia8	585.8
ZGTo2LG_TuneCUETP8M1_13TeV-amcatnloFXFX-pythia8	131.3
TGJets_TuneCUETP8M1_13TeV_amcatnlo_madspin_pythia8	2.967
TGJets_TuneCUETP8M1_13TeV_amcatnlo_madspin_pythia8	2.967
TTGJets_TuneCUETP8M1_13TeV-amcatnloFXFX-madspin-pythia8	3.697
WpWpJJ_EWK-QCD_TuneCUETP8M1_13TeV-madgraph-pythia8	0.03711
ZZZ_TuneCUETP8M1_13TeV-amcatnlo-pythia8	0.01398
WWZ_TuneCUETP8M1_13TeV-amcatnlo-pythia8	0.1651
WZZ_TuneCUETP8M1_13TeV-amcatnlo-pythia8	0.05565
WW_DoubleScattering_13TeV-pythia8	1.64
tZq_ll_4f_13TeV-amcatnlo-pythia8_TuneCUETP8M1	0.0758
ST_tWll_5f_LO_13TeV-MadGraph-pythia8	0.01123
TTTT_TuneCUETP8M1_13TeV-amcatnlo-pythia8	0.009103
WZTo3LNu_TuneCUETP8M1_13TeV-powheg-pythia8	4.4296
ZZTo4L_13TeV_powheg_pythia8	1.256
TTJets_SingleLeptFromTbar_TuneCUETP8M1_13TeV-madgraphMLM-pythia8	182.1754
TTJets_SingleLeptFromT_TuneCUETP8M1_13TeV-madgraphMLM-pythia8	182.1754
TTJets_DiLept_TuneCUETP8M1_13TeV-madgraphMLM-pythia8	87.3
DYJetsToLL_M-10to50_TuneCUETP8M1_13TeV-amcatnloFXFX-pythia8	18610
DYJetsToLL_M-50_TuneCUETP8M1_13TeV-madgraphMLM-pythia8	6024
WJetsToLNu_TuneCUETP8M1_13TeV-amcatnloFXFX-pythia8	61526.7
ST_tW_top_5f_inclusiveDecays_13TeV-powheg-pythia8_TuneCUETP8M1	35.6
ST_tW_antitop_5f_inclusiveDecays_13TeV-powheg-pythia8_TuneCUETP8M1	35.6
ST_t-channel_4f_leptonDecays_13TeV-amcatnlo-pythia8_TuneCUETP8M1	70.3144
ST_t-channel_antitop_4f_leptonDecays_13TeV-powheg-pythia8_TuneCUETP8M1	26.2278
ST_s-channel_4f_leptonDecays_13TeV-amcatnlo-pythia8_TuneCUETP8M1	3.68064
WWTo2L2Nu_13TeV-powheg	10.481

Table 4.3: List of background samples used in this analysis (CMSSW 80X). In the first section of the table are listed the samples of the processes for which we use the simulation to extract the final yields and shapes, in the second section the samples of the processes we will estimate from data. The MC simulation is used to design the data driven methods and derive the associated systematics.

Sample	σ [pb]
ttWJets_13TeV_madgraphMLM	0.6105
ttZJets_13TeV_madgraphMLM	0.5297/0.692

Table 4.4: Leading-order $t\bar{t}W$ and $t\bar{t}Z$ samples used in the signal BDT training.

Three lepton and Four lepton
HLT_DiMu9_Ele9_CaloIdL_TrackIdL_v*
HLT_Mu8_DiEle12_CaloIdL_TrackIdL_v*
HLT_TripleMu_12_10_5_v*
HLT_Ele16_Ele12_Ele8_CaloIdL_TrackIdL_v*
HLT_Mu23_TrkIsoVVL_Ele8_CaloIdL_TrackIdL_IsoVL_v*
HLT_Mu23_TrkIsoVVL_Ele8_CaloIdL_TrackIdL_IsoVL_DZ_v*
HLT_Mu8_TrkIsoVVL_Ele23_CaloIdL_TrackIdL_IsoVL_v*
HLT_Mu8_TrkIsoVVL_Ele23_CaloIdL_TrackIdL_IsoVL_DZ_v*
HLT_Ele23_Ele12_CaloIdL_TrackIdL_IsoVL_DZ_v*
HLT_Mu17_TrkIsoVVL_Mu8_TrkIsoVVL_DZ_v*
HLT_Mu17_TrkIsoVVL_TkMu8_TrkIsoVVL_DZ_v*
HLT_IsoMu22_v*
HLT_IsoTkMu22_v*
HLT_IsoMu22_eta2p1_v*
HLT_IsoTkMu22_eta2p1_v*
HLT_IsoMu24_v*
HLT_IsoTkMu24_v*
HLT_Ele27_WPTight_Gsf_v*
HLT_Ele25_eta2p1_WPTight_Gsf_v*
HLT_Ele27_eta2p1_WPLoose_Gsf_v*

Table 4.5: Table of high-level triggers that we consider in the analysis.

795 Tab. 4.5 shows the lowest-threshold non-preserved triggers present in the High-Level
 796 Trigger (HLT) menus for both Monte-Carlo and data in 2016.

797 **Trigger efficiency scale factors**

798 The efficiency of events to pass the trigger is measured in simulation (trivially using
 799 generator information) and in the data (using event collected by an uncorrelated
 800 MET trigger). Small differences between the data and MC efficiencies are corrected
 801 by applying scale factors as shown in Tab. 4.6. The exact procedure and control plots
 802 are documented in [41] for the current analysis.

Category	Scale Factor
ee	1.01 ± 0.02
e μ	1.01 ± 0.01
$\mu\mu$	1.00 ± 0.01
3l	1.00 ± 0.03

Table 4.6: Trigger efficiency scale factors and associated uncertainties, shown here rounded to the nearest percent.

803 Object Identification and event selection

804 Jets and b tagging

805 The analysis uses anti- k_t (0.4) particle-flow (PF) jets, corrected for charged hadrons
 806 not coming from the primary vertex (charged hadron subtraction), and having jet
 807 energy corrections (`Summer16_23Sep2016V3`) applied as a function of the jet E_T and
 808 η . Jets are only considered if they have a transverse energy above 25GeV.

809 In addition, they are required to be separated from any lepton candidates passing
 810 the fakeable object selections (see Tables 4.7 and 4.8) by $\Delta R > 0.4$.

811 The loose and medium working points of the CSV b-tagging algorithm are used to
 812 identify b jets. Data/simulation differences in the b tagging performance are corrected
 813 by applying per-jet weights to the simulation, dependent on the jet p_T , eta, b tagging
 814 discriminator, and flavor (from simulation truth) [42]. The per-event weight is taken
 815 as the product of the per-jet weights, including those of the jets associated to the
 816 leptons. More details can be found in the corresponding $t\bar{t}H$ documentation [38, 41].

817 Lepton selection

818 The lepton reconstruction and selection is identical to that used in the $t\bar{t}H$ multilepton
 819 analysis, as documented in Refs. [38, 41]. For details on the reconstruction algorithms,

Cut	Loose	Fakeable object	Tight
$ \eta < 2.4$	✓	✓	✓
p_T	$> 5\text{GeV}$	$> 15\text{GeV}$	$> 15\text{GeV}$
$ d_{xy} < 0.05 \text{ (cm)}$	✓	✓	✓
$ d_z < 0.1 \text{ (cm)}$	✓	✓	✓
$\text{SIP}_{3D} < 8$	✓	✓	✓
$I_{\text{mini}} < 0.4$	✓	✓	✓
is Loose Muon	✓	✓	✓
jet CSV	—	< 0.8484	< 0.8484
is Medium Muon	—	—	✓
tight-charge	—	—	✓
lepMVA > 0.90	—	—	✓

Table 4.7: Requirements on each of the three muon selections. In the cases where the cut values change between the selections, those values are listed in the table. Otherwise, whether the cut is applied is indicated. For the two p_T^{ratio} and CSV rows, the cuts marked with a † are applied to leptons that fail the lepton MVA cut, while the loose cut value is applied to those that pass the lepton MVA cut.

820 isolation, pileup mitigation, and a description of the lepton MVA discriminator and
 821 validation plots thereof, we refer to that document since they are out of the scope
 822 of this thesis. Three different selections are defined both for the electron and muon
 823 object identification: the *Loose*, *Fakeable Object*, and *Tight* selection. As described
 824 in more detail later, these are used for event level vetoes, the fake rate estimation
 825 application region, and the final signal selection, respectively. The p_T of fakeable
 826 objects is defined as $0.85 \times p_T(\text{jet})$, where the jet is the one associated to the lepton
 827 object. This mitigates the dependence of the fake rate on the momentum of the
 828 fakeable object and thereby improves the precision of the method.

829 Tables 4.7 and 4.8 list the full criteria for the different selections of muons and
 830 electrons.

Cut	Loose	Fakeable Object	Tight
$ \eta < 2.5$	✓	✓	✓
p_T	$> 7\text{GeV}$	$> 15\text{GeV}$	$> 15\text{GeV}$
$ d_{xy} < 0.05 \text{ (cm)}$	✓	✓	✓
$ d_z < 0.1 \text{ (cm)}$	✓	✓	✓
$\text{SIP}_{3D} < 8$	✓	✓	✓
$I_{\text{mini}} < 0.4$	✓	✓	✓
MVA ID $> (0.0, 0.0, 0.7)$	✓	✓	✓
$\sigma_{i\eta i\eta} < (0.011, 0.011, 0.030)$	—	✓	✓
$\text{H/E} < (0.10, 0.10, 0.07)$	—	✓	✓
$\Delta\eta_{\text{in}} < (0.01, 0.01, 0.008)$	—	✓	✓
$\Delta\phi_{\text{in}} < (0.04, 0.04, 0.07)$	—	✓	✓
$-0.05 < 1/E - 1/p < (0.010, 0.010, 0.005)$	—	✓	✓
p_T^{ratio}	—	$> 0.5 \dagger / -$	—
jet CSV	—	$< 0.3 \dagger / < 0.8484$	< 0.8484
tight-charge	—	—	✓
conversion rejection	—	—	✓
Number of missing hits	< 2	$= 0$	$= 0$
lepMVA > 0.90	—	—	✓

Table 4.8: Criteria for each of the three electron selections. In cases where the cut values change between selections, those values are listed in the table. Otherwise, whether the cut is applied is indicated. In some cases, the cut values change for different η ranges. These ranges are $0 < |\eta| < 0.8$, $0.8 < |\eta| < 1.479$, and $1.479 < |\eta| < 2.5$ and the respective cut values are given in the form (value₁, value₂, value₃).

831 Lepton selection efficiency

832 Efficiencies of reconstruction and selecting loose leptons are measured both for muons
 833 and electrons using a tag and probe method on both data and MC, using $Z \rightarrow \ell^+ \ell^-$.
 834 Corresponding scale factors are derived from the ratio of efficiencies and applied to the
 835 selected These. Events are produced for the leptonic SUSY analyses using equivalent
 836 lepton selections and recycled for the $t\bar{t}H$ analysis as well as for this analysis. The
 837 efficiencies of applying the tight selection as defined in Tables 4.7 and 4.8, on the
 838 loose leptons are determined again by using a tag and probe method on a sample of
 839 DY-enriched events. They are documented for the $t\bar{t}H$ analysis in Ref. [41] and are

840 exactly equivalent for this analysis.

841 Background predictions

842 The modeling of reducible and irreducible backgrounds in this analysis uses the exact
 843 methods, analysis code, and ROOT trees used for the $t\bar{t}H$ multilepton analysis. We
 844 give a brief description of the methods and refer to the documentation of that analysis
 845 in Refs. [38, 41] for any details.

846 The backgrounds in three-lepton final states can be split in two broad categories:
 847 irreducible backgrounds with genuine prompt leptons (i.e. from on-shell W and Z
 848 boson decays); and reducible backgrounds where at least one of the leptons is “non-
 849 prompt”, i.e. produced within a hadronic jet, either a genuine lepton from heavy
 850 flavor decays, or simply mis-reconstructed jets.

851 Irreducible backgrounds can be reliably estimated directly from Monte-Carlo sim-
 852 ulated events, using higher-order cross sections or data control regions for the overall
 853 normalization. This is done in this analysis for all backgrounds involving prompt lep-
 854 tons: $t\bar{t}W$, $t\bar{t}Z$, $t\bar{t}H$, WZ , ZZ , $W^\pm W^\pm qq$, $t\bar{t}t\bar{t}$, tZq , tZW , WWW , WWZ , WZZ ,
 855 ZZZ .

856 Reducible backgrounds, on the other hand, are not well predicted by simulation,
 857 and are estimated using data-driven methods. In the case of non-prompt leptons, a
 858 fake rate method is used, where the contribution to the final selection is estimated by
 859 extrapolating from a sideband (or “application region”) with a looser lepton definition
 860 (the fakeable object definitions in Tabs. 4.7 and 4.8) to the signal selection. The tight-
 861 to-loose ratios (or “fake rates”) are measured in several background dominated data
 862 events with dedicated triggers, subtracting the residual prompt lepton contribution
 863 using MC. Non-prompt leptons in our signal regions are predominantly produced in $t\bar{t}$

864 events, with a much smaller contribution, from Drell–Yan production. The systematic
 865 uncertainty on the normalization of the non-prompt background estimation is on the
 866 order of 50%, and thereby one of the dominant limitations on the performance of
 867 multilepton analyses in general and this analysis in particular. It consists of several
 868 individual sources, such as the result of closure tests of the method using simulated
 869 events, limited statistics in the data control regions due to necessary prescaling of
 870 lepton triggers, and the uncertainty in the subtraction of residual prompt leptons
 871 from the control region.

872 The fake background where the leptons pass the looser selection are weighted
 873 according to how many of them fail the tight criteria. Events with a single failing
 874 lepton are weighted with the factor $f/(1-f)$ for the estimate to the tight selection
 875 region, where f is the fake rate. Events with two failing leptons are given the negative
 876 weight $-f_i f_j / (1 - f_i)(1 - f_j)$, and for three leptons the weight is positive and equal
 877 to the product of $f/(1-f)$ factor evaluated for each failing lepton.

878 Figures 4.2 show the distributions of some relevant kinematic variables, normalized
 879 to the cross section of the respective processes and to the integrated luminosity.

880 Signal discrimination

881 The tHq signal is separated from the main backgrounds using a boosted decision
 882 tree (BDT) classifier, trained on simulated signal and background events. A set of
 883 discriminating variables are given as input to the BDT which produces a output
 884 distribution maximizing the discrimination power. Table 4.9 lists the input variables
 885 used while Figures 4.3 show their distributions for the relevant signal and background
 886 samples, for the three lepton channel. Two BDT classifiers are trained for the two
 887 main backgrounds expected in the analysis: events with prompt leptons from $t\bar{t}W$ and

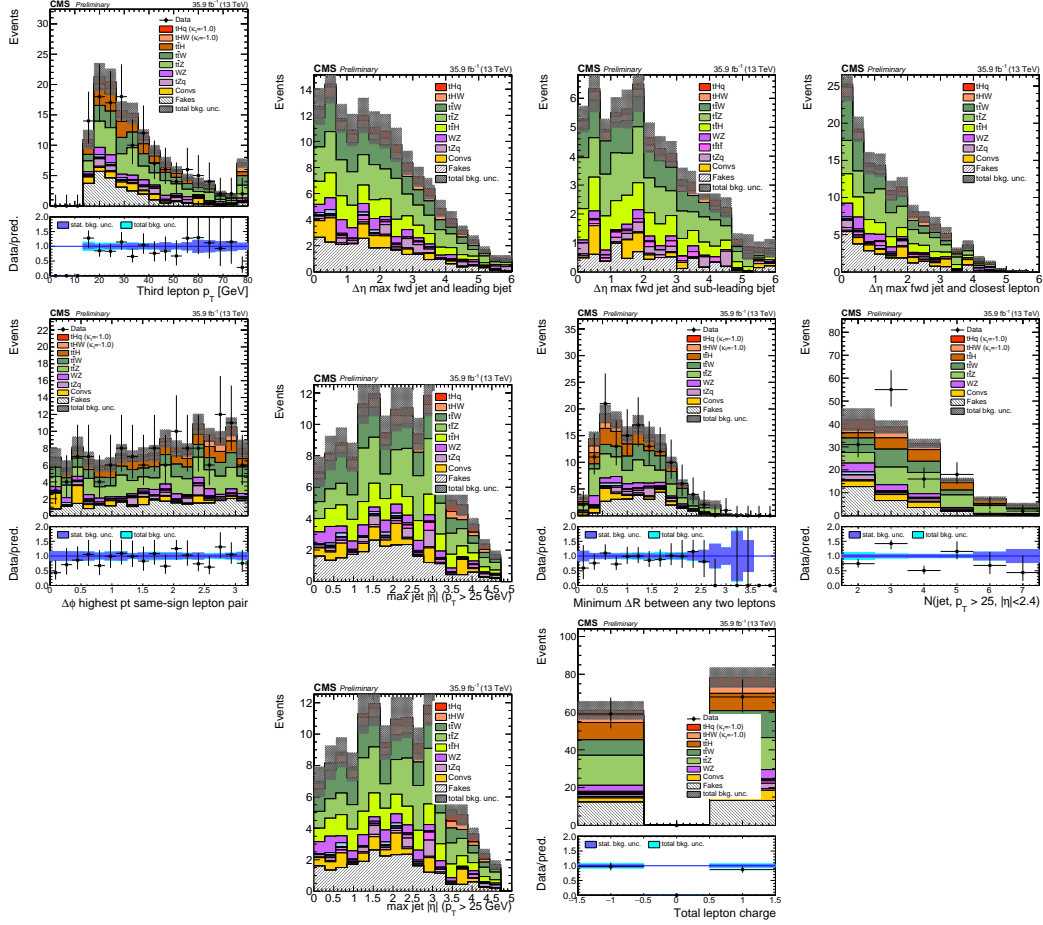


Figure 4.2: Distributions of input variables to the BDT for signal discrimination, three lepton channel, normalized to their cross section and to 35.9fb^{-1} .

888 $t\bar{t}Z$ (also referred to as $t\bar{t}V$), and events with non-prompt leptons from $t\bar{t}$. The datasets
 889 used in the training are the tHq signal (see Tab. 4.1), and LO MADGRAPH samples
 890 of $t\bar{t}W$ and $t\bar{t}Z$, in an admixture proportional to their respective cross sections (see
 891 Tab. 4.4).

892 The MVA analysis consist of two stages: first a “training” where the MVA method
 893 is trained to discriminate between simulated signal and background events, then a
 894 “test” stage where the trained algorithm is used to classify different events from
 895 the samples. The sample is obtained from a pre-selection (see Tab. ?? with pre-
 896 selection cuts). Figures 4.4 show the input variables distributions as seen by the

Variable name	Description
nJet25	Number of jets with $p_T > 25$ GeV, $ \eta < 2.4$
MaxEtaJet25	Maximum $ \eta $ of any (non-CSV-loose) jet with $p_T > 25$ GeV
totCharge	Sum of lepton charges
nJetEta1	Number of jets with $ \eta > 1.0$, non-CSV-loose
detaFwdJetBJet	$\Delta\eta$ between forward light jet and hardest CSV loose jet
detaFwdJet2BJet	$\Delta\eta$ between forward light jet and second hardest CSV loose jet (defaults to -1 in events with only one CSV loose jet)
detaFwdJetClosestLep	$\Delta\eta$ between forward light jet and closest lepton
dphiHighestPtSSPair	$\Delta\phi$ of highest p_T same-sign lepton pair
minDRll	minimum ΔR between any two leptons
Lep3Pt/Lep2Pt	p_T of the 3 rd lepton (2 nd for ss2l)

Table 4.9: MVA input discriminating variables

897 MVA algorithm. Note that in contrast to the distributions in Fig. 4.3 only the main
 898 backgrounds ($t\bar{t}$ from simulation, $t\bar{t}V$) are included.

899 Note that splitting the training in two groups reveals that some variables show
 900 opposite behavior for the two background sources; potentially screening the discrimi-
 901 nation power if they were to be used in a single discriminant. For some other variables
 902 the distributions are similar in both background cases.

903 From table 4.9, it is clear that the input variables are correlated to some extend.
 904 These correlations play an important role for some MVA methods like the Fisher
 905 discriminant method in which the first step consist of performing a linear transfor-
 906 mation to an phase space where the correlations between variables are removed. In
 907 case a boosted decision tree (BDT) method however, correlations do not affect the
 908 performance. Figure 4.6 show the linear correlation coefficients for signal and back-
 909 ground for the two training cases (the signal values are identical by construction). As
 910 expected, strong correlations appears for variables related to the forward jet activity.
 911 Same trend is seen in case of the same sign dilepton channel in Figure ??.

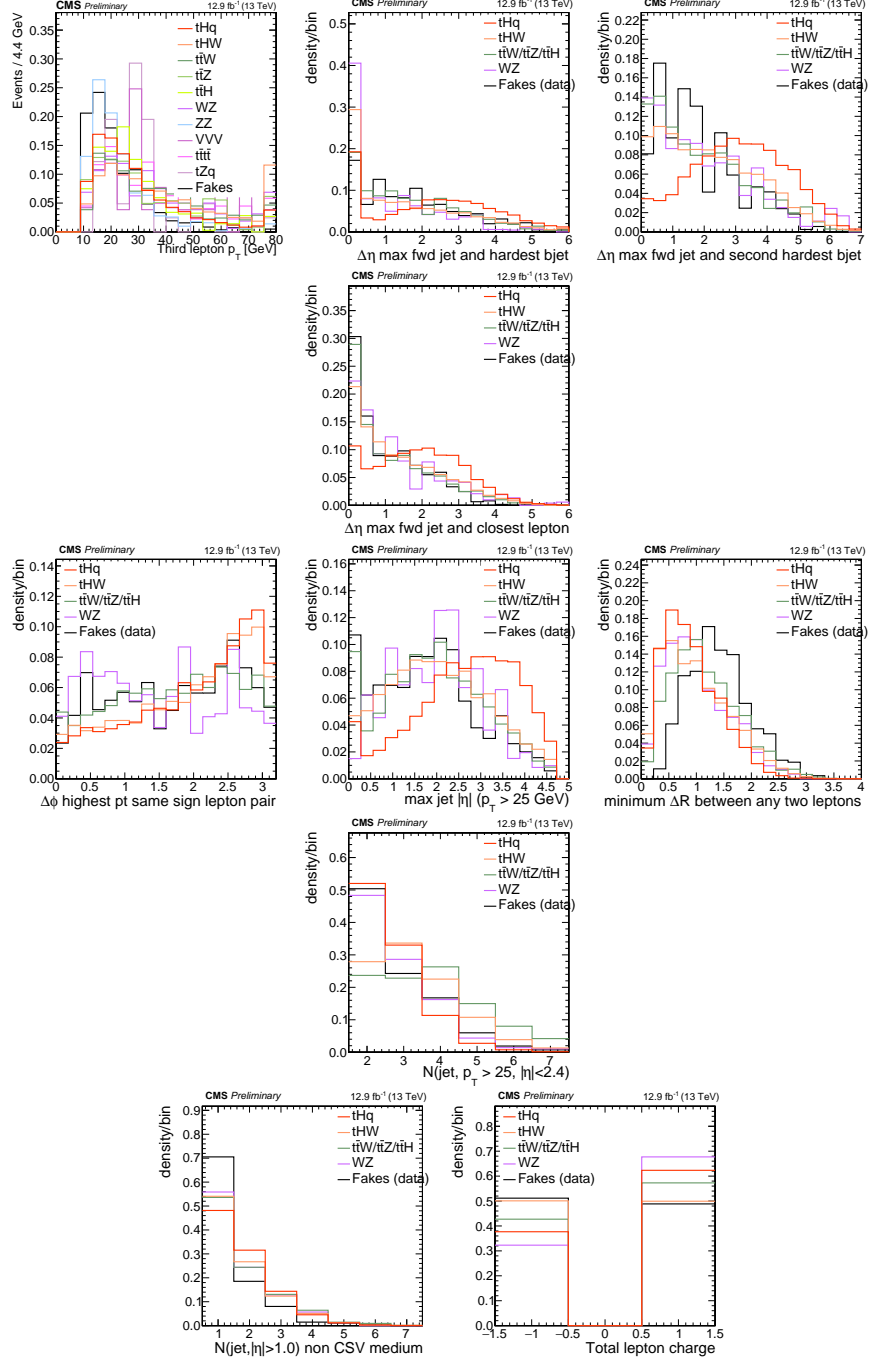


Figure 4.3: Distributions of input variables to the BDT for signal discrimination, three lepton channel.

912 Classifiers response

913 Several MVA algorithms were evaluated to determine the most appropriate method

914 for this analysis. The plots in Fig. 4.7 (top) show the background rejection as a

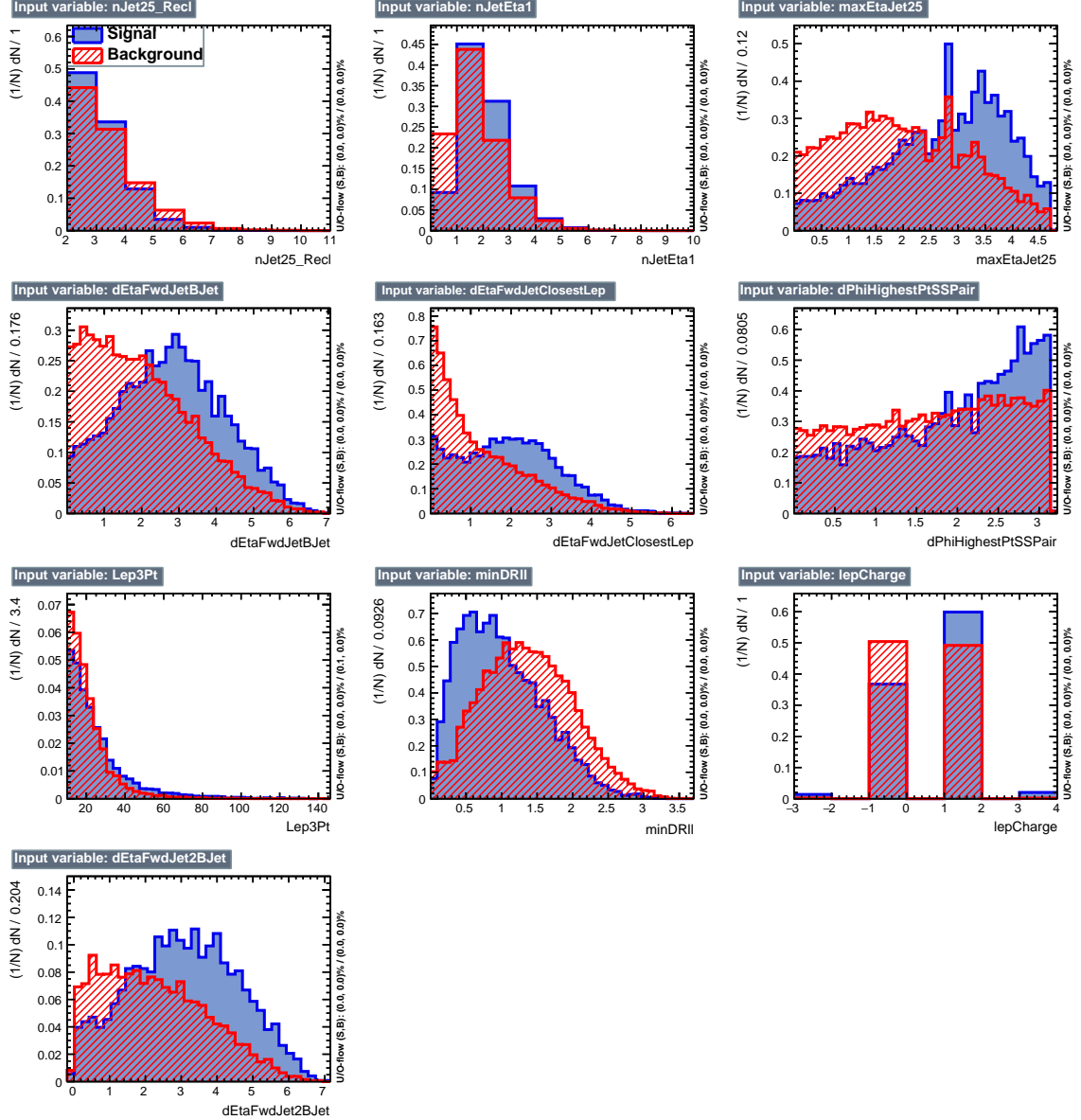


Figure 4.4: BDT inputs as seen by TMVA (signal, in blue, is tHq , background, in red, is $t\bar{t}$) for the three lepton channel, discriminated against $t\bar{t}$ (fakes) background.

function of the signal efficiency for $t\bar{t}$ and $t\bar{t}V$ trainings (ROC curves) for the different algorithms that were evaluated.

In both cases the gradient boosted decision tree (“BDTA_GRAD”) classifier offers the best results, followed by an adaptive BDT classifier (“BDTA”). The BDTA_GRAD classifier output distributions for signal and backgrounds are shown on the bottom of

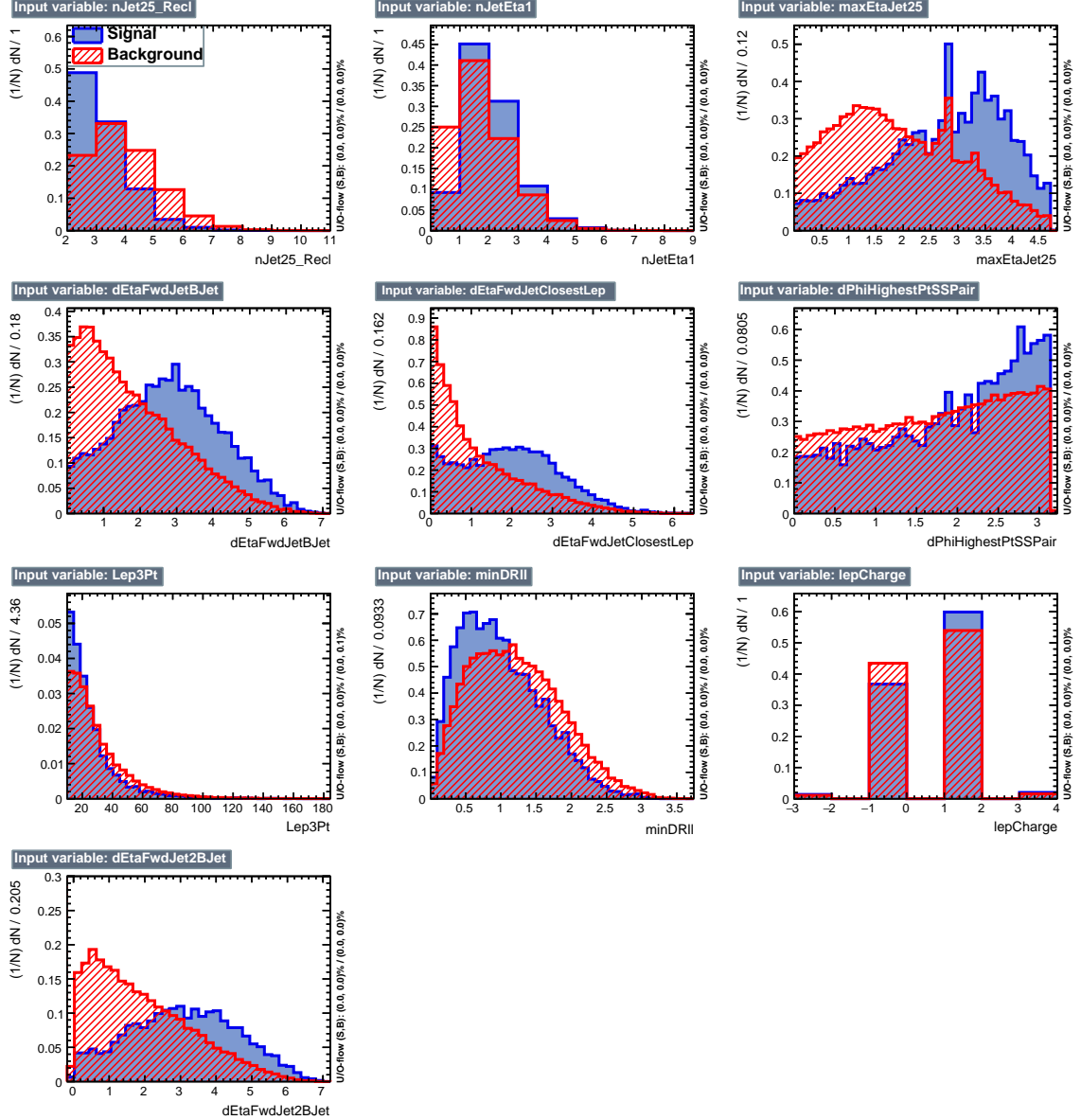


Figure 4.5: BDT inputs as seen by TMVA (signal, in blue, is tHq , background, in red, is $t\bar{t}W+t\bar{t}Z$) for the three lepton channel, discriminated against $t\bar{t}V$ background.

Fig. 4.7. As expected, a good discrimination power is obtained using default discriminator parameter values, with minimal overtraining. TMVA provides a ranking of the input variables by their importance in the classification process, shown in Tab. 4.10. The TMVA settings used in the BDT training are shown in Tab. 4.11.

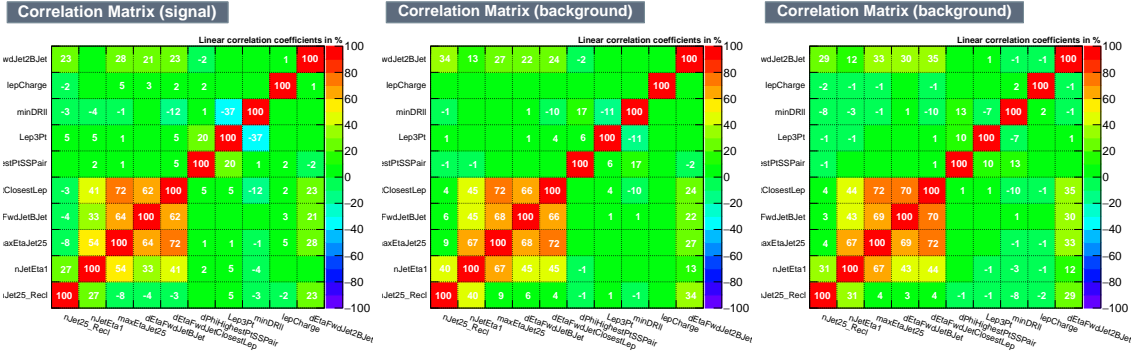


Figure 4.6: Signal (left), $t\bar{t}$ background (middle), and $t\bar{t}V$ background (right.) correlation matrices for the input variables in the TMVA analysis for the three lepton channel.

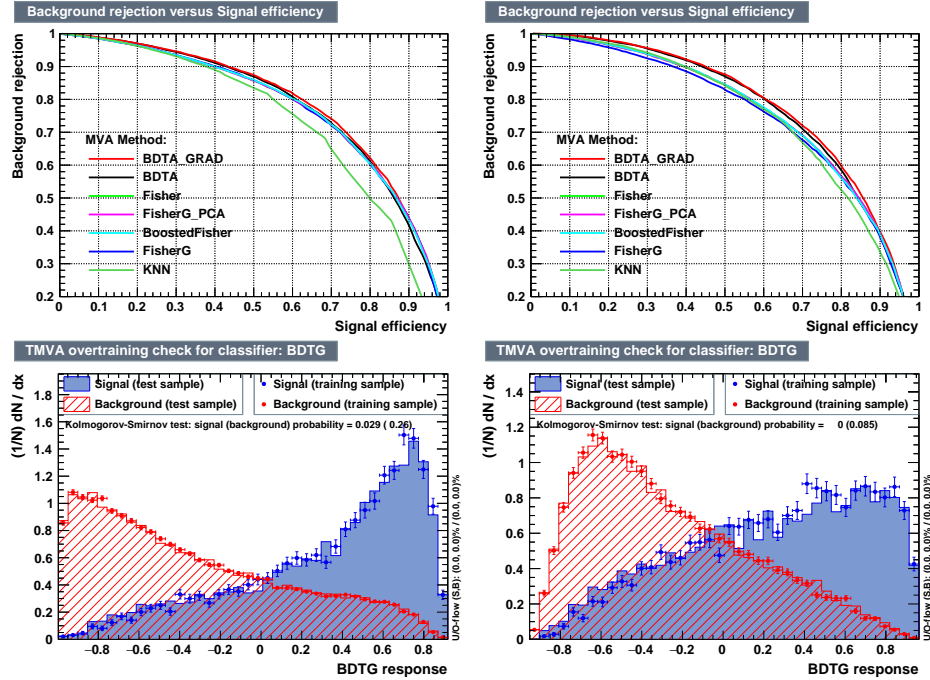


Figure 4.7: Top: background rejection vs signal efficiency (ROC curves) for various MVA classifiers (top) in the three lepton channel against $t\bar{t}V$ (left) and $t\bar{t}$ (right). Bottom: classifier output distributions for the gradient boosted decision trees, for training against $t\bar{t}V$ (left) and against $t\bar{t}$ (right).

924 Additional discriminating variables

925 Two additional discriminating variables were tested considering the fact that the
926 forward jet in the background could come from the pileup; since we have a real

ttbar training			ttV training		
Rank	Variable	Importance	Variable	Importance	
1	minDRll	1.329e-01	dEtaFwdJetBJet	1.264e-01	
2	dEtaFwdJetClosestLep	1.294e-01	Lep3Pt	1.224e-01	
3	dEtaFwdJetBJet	1.209e-01	maxEtaJet25	1.221e-01	
4	dPhiHighestPtSSPair	1.192e-01	dEtaFwdJet2BJet	1.204e-01	
5	Lep3Pt	1.158e-01	dEtaFwdJetClosestLep	1.177e-01	
6	maxEtaJet25	1.121e-01	minDRll	1.143e-01	
7	dEtaFwdJet2BJet	9.363e-02	dPhiHighestPtSSPair	9.777e-02	
8	nJetEta1	6.730e-02	nJet25_Recl	9.034e-02	
9	nJet25_Recl	6.178e-02	nJetEta1	4.749e-02	
10	lepCharge	4.701e-02	lepCharge	4.116e-02	

Table 4.10: TMVA input variables ranking for BDTA_GRAD method for the trainings in the three lepton channel. For both trainings the rankings show almost the same 5 variables in the first places.

```
TMVA.Types.kBDT
NTrees=800
BoostType=Grad
Shrinkage=0.10
!UseBaggedGrad
nCuts=50
MaxDepth=3
NegWeightTreatment=PairNegWeightsGlobal
CreateMVAPdfs
```

Table 4.11: TMVA configuration used in the BDT training.

927 forward jet in the signal, it could give some improvement in the discriminating power.
 928 The additional variables describe the forward jet momentum (fwdJetPt25) and the
 929 forward jet identification(fwdJetPUID). Distributions for these variables in the three
 930 lepton channel are shown in the figure 4.8. The forward jet identification distribution
 931 show that for both, signal and background, jets are mostly real jets.

932 The testing was made including in the MVA input one variable at a time, so we
 933 can evaluate the dicrimination power of each variable, and then both simultaneously.
 934 fwdJetPUID was ranked in the last place in importance (11) in both training (ttV
 935 and tt) while fwdJetPt25 was ranked 3 in the ttV training and 7 in the tt training.

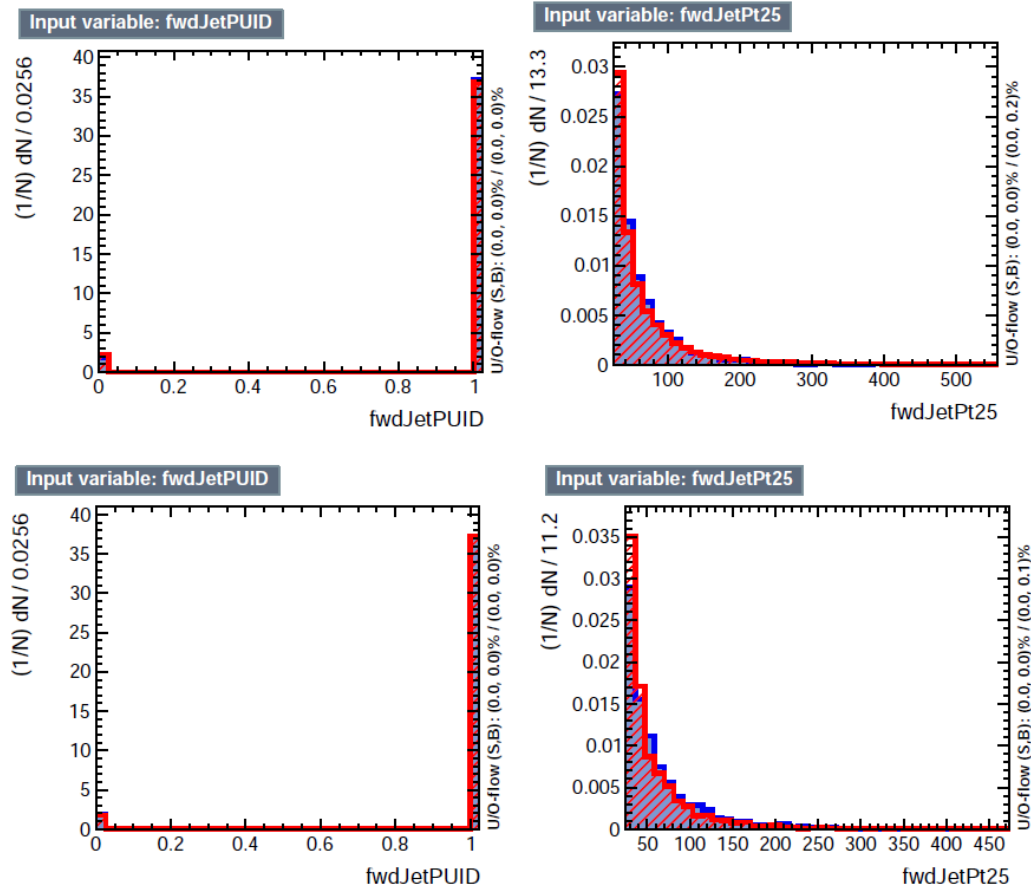


Figure 4.8: Additional discriminating variables distributions for ttv training (Top row) and tt training (bottom row) in the three lepton channel. The origin of the jets in the forward jet identification distribution is tagged as 0 for “pileup jets” while “real jets” are tagged as 1.

936 When training using 12 variables, `fwdJetPt25` was ranked 5 and 7 in the ttV and tt
937 trainings respectively, while `fwdJetPUID` was ranked 12 in both cases.

938 The improvement in the discrimination performance provided by the additional
939 variables is about 1%, so it was decided not to include them in the procedure. Table
940 4.12 show the ROC-integral for all the testing cases we made.

ROC-integral	
base 10 var ttv	0.848
+ fwdJetPUID ttv	0.849
+ fwdJetPt25 ttv	0.856
12 var ttv	0.856
<hr/>	
base 10 var tt	0.777
+ fwdJetPUID tt	0.777
+ fwdJetPt25 tt	0.787
12 var	0.787

Table 4.12: ROC-integral for all the testing cases we made in the evaluation of the additional variables discriminating power. The improvement in the discrimination performance provided by the additional variables is about 1%

941 Chapter 5

942 The CMS forward pixel detector

943 The phase 1 FPix upgrade

944 FPix module production line

945 The Gluing stage

946 The Encapsulation stage

947 The FPix module production yields

948 References

- 949 [1] A. Einstein “Über einen die Erzeugung und Verwandlung des Lichtes betref-
 950 fenden heuristischen Gesichtspunkt”. Annalen der Physik. 17 (6): 132–148,
 951 (1905).
- 952 [2] A. Einstein. “Über die von der molekularkinetischen Theorie der Wärme
 953 geforderte Bewegung von in ruhenden Flüssigkeiten suspendierten Teilchen”.
 954 Annalen der Physik. 17 (8): 549–560, (1905).
- 955 [3] A. Einstein. “Zur Elektrodynamik bewegter Körper”. Annalen der Physik. 17
 956 (10): 891–921, (1905).
- 957 [4] A. Einstein, “Ist die Trägheit eines Körpers von seinem Energieinhalt ab-
 958 hängig?”. Annalen der Physik. 18 (13): 639–641, (1905).
- 959 [5] S. Tomonaga. “On a Relativistically Invariant Formulation of the Quantum
 960 Theory of Wave Fields”. Progress of Theoretical Physics. 1 (2): 27–42, (1946).
- 961 [6] J. Schwinger. “Quantum Electrodynamics. I. A Covariant Formulation”. Phys-
 962 ical Review. 74 (10): 1439–61, (1948).
- 963 [7] R. P. Feynman. “Space-Time Approach to Quantum Electrodynamics”.
 964 Physical Review. 76 (6): 769–89, (1949).

- 965 [8] S.L. Glashow. “Partial symmetries of weak interactions”, Nucl. Phys. 22 579-
966 588, (1961).
- 967 [9] A. Salam, J.C. Ward. “Electromagnetic and weak interactions”, Physics Letters
968 13 168-171, (1964).
- 969 [10] S. Weinberg, “A model of leptons”, Physical Review Letters, vol. 19, no. 21, p.
970 1264, (1967).
- 971 [11] E. Noether, “Invariante Variationsprobleme”, Nachrichten von der Gesellschaft
972 der Wissenschaften zu GÃ¶ttingen, mathematisch-physikalische Klasse, vol.
973 1918, pp. 235â€¢257, (1918).
- 974 [12] M. Goldhaber, L. Grodzins, A.W. Sunyar “Helicity of Neutrinos”, Phys. Rev.
975 109, 1015 (1958).
- 976 [13] Palanque-Delabrouille N et al. “Neutrino masses and cosmology with Lyman-
977 alpha forest power spectrum”, JCAP 11 011 (2015).
- 978 [14] M. Gell-Mann. “A Schematic Model of Baryons and Mesons”. Physics Letters.
979 8 (3): 214â€¢215 (1964).
- 980 [15] G. Zweig. “An SU(3) Model for Strong Interaction Symmetry and its Breaking”
981 (PDF). CERN Report No.8182/TH.401 (1964).
- 982 [16] G. Zweig. “An SU(3) Model for Strong Interaction Symmetry and its Breaking:
983 II” (PDF). CERN Report No.8419/TH.412(1964).
- 984 [17] M. Gell-Mann. “The Interpretation of the New Particles as Displaced Charged
985 Multiplets”. Il Nuovo Cimento 4: 848. (1956).

- 986 [18] T. Nakano, K, Nishijima. “Charge Independence for V-particles”. Progress of
987 Theoretical Physics 10 (5): 581-582. (1953).
- 988 [19] File:Weak Decay (flipped).svg. (2017, June 12). Wikimedia Com-
989 mons, the free media repository. Retrieved 19:13, November 27, 2017
990 from [https://commons.wikimedia.org/w/index.php?title=File:Weak_Decimal_\(flipped\).svg&oldid=247498592](https://commons.wikimedia.org/w/index.php?title=File:Weak_Decimal_(flipped).svg&oldid=247498592).
- 992 [20] N. Cabibbo, “Unitary symmetry and leptonic decays” Physical Review Letters,
993 vol. 10, no. 12, p. 531, (1963).
- 994 [21] M.Kobayashi, T.Maskawa, “CP-violation in the renormalizable theory of weak
995 interaction,” Progress of Theoretical Physics, vol. 49, no. 2, pp. 652-657, (1973).
- 996 [22] M. Peskin, D. Schroeder, “An introduction to quantum field theory”. Perseus
997 Books Publishing L.L.C., (1995).
- 998 [23] F. Mandl, G. Shaw. “Quantum field theory.” Chichester: Wiley (2009).
- 999 [24] F. Halzen, and A.D. Martin, “Quarks and leptons: An introductory course in
1000 modern particle physics”. New York: Wiley, (1984) .
- 1001 [25] A. Pich. “The Standard Model of Electroweak Interactions”
1002 <https://arxiv.org/abs/1201.0537>
- 1003 [26] F.Bellaiche. (2012, 2 September). “What’s this Higgs boson anyway?”. Retrieved
1004 from: <https://www.quantum-bits.org/?p=233>
- 1005 [27] M. Endres et al. Nature 487, 454-458 (2012) doi:10.1038/nature11255

- 1006 [28] F. Englert, R. Brout. “Broken Symmetry and the Mass of Gauge Vect-
 1007 tor Mesons”. Physical Review Letters. 13 (9): 321–323.(1964) Bib-
 1008 code:1964PhRvL..13..321E. doi:10.1103/PhysRevLett.13.321
- 1009 [29] P.Higgs. “Broken Symmetries and the Masses of Gauge Bosons”. Physical
 1010 Review Letters. 13 (16): 508–509,(1964). Bibcode:1964PhRvL..13..508H.
 1011 doi:10.1103/PhysRevLett.13.508.
- 1012 [30] G.Guralnik, C.R. Hagen and T.W.B. Kibble. “Global Conservation Laws and
 1013 Massless Particles”. Physical Review Letters. 13 (20): 585–587, (1964). Bib-
 1014 code:1964PhRvL..13..585G. doi:10.1103/PhysRevLett.13.585.
- 1015 [31] CMS collaboration. “Observation of a new boson at a mass of 125
 1016 GeV with the CMS experiment at the LHC”. Physics Letters B.
 1017 716 (1): 30–61 (2012). arXiv:1207.7235. Bibcode:2012PhLB..716...30C.
 1018 doi:10.1016/j.physletb.2012.08.021
- 1019 [32] ATLAS collaboration. “Observation of a New Particle in the Search for
 1020 the Standard Model Higgs Boson with the ATLAS Detector at the LHC”.
 1021 Physics Letters B. 716 (1): 1–29(2012). arXiv:1207.7214. Bib-
 1022 code:2012PhLB..716....1A. doi:10.1016/j.physletb.2012.08.020.
- 1023 [33] ATLAS collaboration; CMS collaboration (26 March 2015). “Combined
 1024 Measurement of the Higgs Boson Mass in pp Collisions at $\sqrt{s}=7$ and
 1025 8 TeV with the ATLAS and CMS Experiments”. Physical Review Let-
 1026 ters. 114 (19): 191803. arXiv:1503.07589. Bibcode:2015PhRvL.114s1803A.
 1027 doi:10.1103/PhysRevLett.114.191803.
- 1028 [34] CMS Collaboration, “SM Higgs Branching Ratios and To-
 1029 tal Decay Widths (up-date in CERN Report4 2016)”.

- 1030 <https://twiki.cern.ch/twiki/bin/view/LHCPhysics/CERNYellowReportPageBR>
 1031 , last accessed on 17.12.2017.
- 1032 [35] C. Patrignani et al. (Particle Data Group), Chin. Phys. C, 40, 100001 (2016)
 1033 and 2017 update.
- 1034 [36] CMS Collaboration, “Search for the associated production of a Higgs boson
 1035 with a single top quark in proton-proton collisions at $\sqrt{s} = 8$ TeV”, JHEP 06
 1036 (2016) 177, doi:10.1007/JHEP06(2016)177, arXiv:1509.08159.
- 1037 [37] B. Stieger, C. Jorda Lope et al., “Search for Associated Production of a Single
 1038 Top Quark and a Higgs Boson in Leptonic Channels”, CMS Analysis Note CMS
 1039 AN-14-140, 2014.
- 1040 [38] M. Peruzzi, C. Mueller, B. Stieger et al., “Search for ttH in multilepton final
 1041 states at $\sqrt{s} = 13$ TeV”, CMS Analysis Note CMS AN-16-211, 2016.
- 1042 [39] CMS Collaboration, “Search for H to bbar in association with a single top quark
 1043 as a test of Higgs boson couplings at $\sqrt{s} = 13$ TeV”, CMS Physics Analysis
 1044 Summary CMS-PAS-HIG-16-019, 2016.
- 1045 [40] B. Maier, “SingleTopHiggProduction13TeV”, February, 2016.
 1046 <https://twiki.cern.ch/twiki/bin/viewauth/CMS/SingleTopHiggsGeneration13TeV>.
- 1047 [41] M. Peruzzi, F. Romeo, B. Stieger et al., “Search for ttH in multilepton final
 1048 states at $\sqrt{s} = 13$ TeV”, CMS Analysis Note CMS AN-17-029, 2017.
- 1049 [42] B. WG, “BtagRecommendation80XReReco”, February, 2017.
 1050 <https://twiki.cern.ch/twiki/bin/view/CMS/BtagRecommendation80XReReco>.